BILINGUAL PUBLISHING GROUP

Journal of Building Material Science

Volume 5 • Issue 1 • June 2023 ISSN 2630-5216(Online)

Volume 5 Issue 1 • June 2023 • ISSN 2630-5216 (Online)

JOURNAL OF BUILDING MATERIAL SCIENCE

BILINGUAL PUBLISHING GROUP

BILINGUAL PUBLISHING GROUP

Volume 5 | Issue 1 | June 2023 | Page1-54

Journal of Building Material Science

Contents

Editorial

Articles

BILINGUAL PUBLISHING GROUP

Journal of Building Material Science

https://journals.bilpubgroup.com/index.php/jbms

ARTICLE

Novel Proposal of Bio-based Sewing Timber Joint: Learning from Diatoms

***Mauricio Díaz Valdés*[1*], *Melisa Gálvez Bohórquez*[2]**

[1] *Parametric Design, Polytechnic University of Catalonia, Carrer de Pere Serra, 1, Sant Cugat del Vallès, Barcelona, 08034, Spain*

[2] *Faculty of architecture, University of La Gran Colombia, Bogotá, 110110, Colombia*

ABSTRACT

The twenty-first century is one of the most complex in the history of humanity, mainly due to the ecological crisis it is going through. The construction sector generates about 40% of CO_2 emissions into the environment; the foregoing should motivate this sector to seek new alternatives to develop new building practices. Taking these current needs into account, this document classifies and presents a multidisciplinary solution that integrates biology, engineering and architecture to develop a new and innovative lightweight timber structure; it divides with a main structure made of timber and an innovative joint system made of bio-polymers connecting all the panels. Through the study of diatoms, it was able to analyze the bio-morphology of the structure, joints and in particular the geometry since they were the inspiration for the design of this structure that presents an innovative and novel design of structural optimization. Through parametric design and digital fabrication, it was able to create a complex geometry that obtains excellent structural behavior. This research discusses and explores how materials, geometry led to the optimization of a structure and how new structures can arise, thanks to biology new solutions can be obtained that are completely sustainable, being a clear example of how to combat the effects of the climate change and in a precise way it highlights the advantages of the bio-design in the architectural design.

Keywords: Diatoms; Timber joinery; Computational method; Topology optimization; Biomimetics; Bio-inspired; Lightweight structure

1. Introduction

The current environmental crisis and the increase in demand for new buildings put the construction sector with many challenges that must find new solutions

*CORRESPONDING AUTHOR:

Mauricio Díaz Valdés, Parametric Design, Polytechnic University of Catalonia, Carrer de Pere Serra, 1, Sant Cugat del Vallès, Barcelona, 08034, Spain; Email: mdiaz@acier.com.mx

ARTICLE INFO

Received: 2 December 2022 | Revised: 12 January 2023 | Accepted: 8 February 2023 | Published Online: 20 February 2023

DOI: https://doi.org/10.30564/jbms.v5i1.5299

CITATION

Valdés, M.D., Bohórquez, M.G., 2023. Novel Proposal of Bio-based Sewing Timber Joint: Learning from Diatoms. Journal of Building Material Science. 5(1): 1-8. DOI: https://doi.org/10.30564/jbms.v5i1.5299

to face climate change since the construction sector is responsible for about a third of emissions, dominated merely by the manufacture of materials such as concrete and steel; this should motivate this sector to seek new alternatives for construction practices and techniques that drive a new way of designing. Changing current conventional construction practices to new ways of innovating structures through timber represents a sustainable alternative in the construction industry. Timber as a construction material has great advantages over other materials, not only for its ecological benefits but also for its negative carbon footprint and its hardness to generate shapes, another great advantage is that it is much cheaper when compared to other materials of construction. If it is able to manage to apply the technological advances that currently exist, construction using timber provides new possibilities and the development of new innovative and sustainable structures.

Through the technological and scientific advances that have been developed during the last decades, being more precise in software and digital fabrication, new structures are being obtained that have greater and better structural performance. Referring to the above and applied to lightweight timber structures, they promise new construction systems; the application materials that are environmentally friendly allow those new lightweight structures could be designed and fabricated very quickly; that's why the interest in timber structures is growing really fast because of their low construction price, material price, high durability and usability.

This present document is the result of the cooperation, knowledge and research of biologists, engineers, architects and builders; with the multidisciplinary perspective, a better result can be obtained for the elaboration of this project; through the combination of knowledge from these areas, it was possible to create a structure that promoted a light and sustainable structure. This research was possible thanks to a research stay at the Institute of Biology and the Faculty of Engineering of both the National Autonomous University of Mexico and the University of La Gran Colombia in Bogota, Colombia.

The objective of biomimicry in architecture is to innovate through biological principles. The purpose of investigating areas is to denote and limit that they are completely different from one another and cannot be compared to a living organism; the important thing to highlight is how you can try to integrate biological principles (geometry, shapes, processes) and integrate them into architectural design. The fields in architecture where it can be applied are diverse and that is why during the last decades, they have been gaining more interest in this sector. In order to carry out this research, a study of several species of *phytoplankton* was carried out and due to their great ecological contribution and geometric principles; that's why for this research it was decided to study diatoms and to be focused on their bio-morphology in order to develop new methods and implement them and as for the design of the joints, as a great result to carry it with sewing joints made of biopolymers, resulting in a new innovative form of construction systems.

The methodology that was used to verify this research is focused on carrying out an investigation at the Institute of Biology, in which it was carried out different analyzes of *phytoplankton*; continued with the development of different design prototypes in which we sought the most suitable geometric shape and for the last part of the conclusion it was with the tests at the Institute of Engineering to carry out the mechanical tests of the bio-polymers. It is important to note that the methodology used was done in different hierarchies; starting first with the analysis that is focused on bio-mimesis and later, the transfer of the geometric shape to the timber panels was carried out so that at the end of this research, it carried out the sewn tests of the biopolymer joints. Due to the above and it should be noted that this investigation has a highly multidisciplinary perspective which helped to obtain a better result.

This prototype is planned to be carried out in an ecological park in Mexico abroad, if compared to a steel and concrete structure, wood has great advantages such as price, time and duration. Regarding maintenance, if it is given a layer of varnish for exterior use, it can withstand the weather and rain, which gives it much greater advantages and is a highly sustainable material.

2. Aim of this research

This document has the purpose of making known how new structures can be developed through the integration of biological principles and how a multi-disciplinary perspective can achieve a better result. The objective of the research is to introduce a new sustainable timber joint union-made of bio-polymers. One of the reasons to develop and apprises this research is that has the purpose of making known how the morphological and biological principles can be an option to develop new lightweight structures. This research concludes with the fabrication of this model and we conclude that it presents great advantages over conventional steel and cement structures. The urgency of designing new construction systems and integrating new materials is one of the main goals for the future of architecture.

3. Diatoms and bio-inspired design

The use of nature in the design process of structures is not something new, it has been applied for several years and day to day it seeks to further expand [1] this knowledge due to the great developments that have been generated in the last decades; in the case of design, it promotes solutions and the development of new designs that integrate new materials and optimal structural forms. During the 20th century, great pioneers of lightweight structures such as Félix Candela, Frei Otto and Fuller Buckminster used biological principles [2] to develop their works and referring to Fuller Buckminster he stated: "I am not trying to imitate nature, I am trying to discover and employ the principles she is using", denoting how nature and biology have much to teach us. During the last century Frei Otto became very interested in biology [3] and it was thus that he worked in collaboration with the biologist J.G. Helmke, being highly interested in *Radiolaria* microorganisms (group of amoeboid protists that produce mineral skeletons) due to their geometry and their structural patterns to develop a balance of light structures. For this emerged his theory, that so-called "From-Finding", which led to his analogic models, like chains or nets of cables [4].

For this research and due to its great interest, we decided to study the diatoms, which are a group of unicellular algae that are part of the *phytoplankton* family, they are photo-synthesizing microorganisms. Most of the oxygen is produced through the *photosynthesis* of *phytoplankton* in the sea, one of which is the diatom, a unicellular alga considered the main generator of oxygen on our planet, so far more than 6 thousand species are known. The function of diatoms in the world's oceans is of great importance since they exhale more oxygen than all the tropical forests of the world and on the other hand, they invisibly recycle the gases that surround our planet. Currently diatoms are considered the "lungs" of the earth since they help to a large extent to be able to produce oxygen and absorb large amounts of CO_2.

Apart from their great contributions to the ecology and well-being of the planet, diatoms have great characteristics linked to their bio-morphology, especially for this research will focus on the shape and geometry that makes them have completely precise geometric shapes. After several analyzes of different diatoms and different species of *phytoplankton*, we concluded that the best species to continue with the analysis of this structure would be two species: *Triceratium Favus* and *Coscindiscus Radiautus* (**Figure 1**). The first one has a completely equilateral triangle shape; under these geometric principles it was chosen to use this species to design the main structure that has an inner radius and three support points in the same way and this benefits structural optimization. The second species has a hexagonal shape. This is the base of the timber membrane that was developed to optimize the main membrane (**Figure 2**).

On the left side the *Triceratium Favus* has a completely triangular structure and on the right side the hexagons that make up the *Coscindiscus Radiautus*, both being observed under a microscope. Learning through morphology and biological principles and applying them to construction is a tradition that has been applied for several years now; but lately it has generated greater because of the endless opportunities and possibilities that give a plus to the design process. In

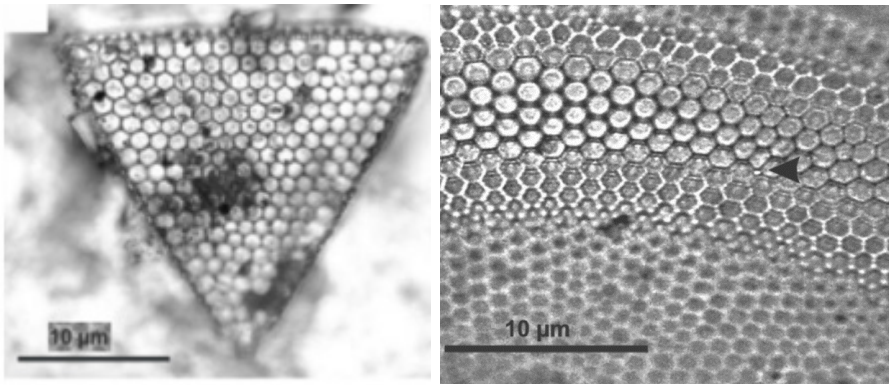

Figure 1. *Phytoplankton* view through a microscope.

the case of the field of lightweight timber structures, biological principles and morphology have helped redefine construction systems [5], construction methodologies, architectural design, and fabrication processes. On the other hand, the great dilemma is based on how to transfer these biological principles to the construction process; these challenges are the crucial part that motivates us to develop innovative solutions and integrate new design methodologies.

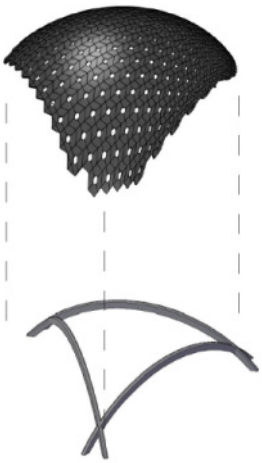

Figure 2. Pavilion divisions.

3.1 Joint connections

One of the essential aspects of any structure is the connections since they are responsible for transferring all the forces, in the case of timber construction there are different types of connections that go from the joints connected with glue, screw and nuts; we chose to integrate biopolymers to develop the sewing joints of each of the panels.

The sewing joints present a great direct opportunity for the union of each one of the panels of the membrane, since it allows the direct transfer of each one of the panels [6], this type of union has already been used in other architectural works, but in the case of this structure, a bio-polymer is used that allows it to be sustainable and rigid at the same time. After the parametric design of the structure, carrying out the tests in the Karamba plug-in, showing behavior and a minimum displacement with the design of the sandwich-type joined panels. The innovation of this structure is that it also has the benefit of being highly adaptable to any geometry or surface and that it can be tensioned correctly, making it a great contribution to the design of lightweight structures.

As a result of the flexible joints, it is able to develop any type of surface and it can be built. In the case of the project carried out, the structural behavior promotes the development of new forms that can be adapted to any design need. This structural behavior is a great advantage compared to concrete and steel structures. Sewing joints present a great promising future since compared to steel or concrete they present great economic and sustainable advantages [7]. In the case of the project presented, each hexagon is connected through this system (**Figure 3**). The goal of this system is to apply new low-tech construction systems by means of timber and sewing joints for the manufacture of lightweight structures and to explore the tension, compression and elasticity of this structure.

Detail of the sewing joint system; the sewn joint is made in the middle of each panel leaving an overlap of 5 centimeters. This allows for an adaptation of the hexagons to any surface. The thickness of the plywood is 1.5 mm. The different test was done and

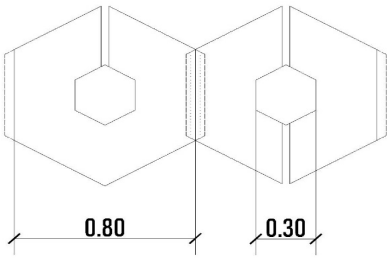

Figure 3. Joint connection between panels.

carried out several samples to be able to know the shear and the stress that these joints could handle. These samples with the sewing machine and different types of joints were tested; through experimentation we came to the conclusion that joints that are overlapped are the best option to be able to transfer loads through the surface **(Figure 4**). Making a reference to the biopolymer, different tests were carried out to find out its resistance and we compared it with a steel cable in which the resistance of the steel cable is greater than 1200 kilos but in the case of the biopolymer its breaking point was 680 kilos (**Graph 1**), which places it as a sustainable proposal and with different experiments we can generate new proposals with this material and increase its resistance.

Figure 4. Sewing process of the timber.

3.2 Material and fabrication

For several centuries, timber has been one of the most important construction materials and due to its great sustainability and economic contributions that's why it was used or the main structure and hexagon panels; in the case of biopolymers, they are gaining ground due to its mechanical and structural properties that they promote. It should be noted that the time that infers humanity currently demands analyzing and seeking solutions with a multidisciplinary perspective in order to carry out and generate a better result in the face of the adversities of climate change.

However, the progress during the last decades in digital fabrication, software and new materials has benefited from new possibilities and opportunities of bio-design for architecture and construction, promoting the design of optimal complex geometries. On the other hand, the integration of biology into architecture allows us to better study and understand how to address problems and generate new solutions. Especially in the field of lightweight timber construction, biological role models have helped to redefine building systems, design methodologies, and fabrication technologies.

This research presents the design of an experimental structure that was made in timber and biopolymers for the joints. These materials have a lot of great interest due to their biodegradability, low cost and mechanical properties. In the case of biopolymers have great advantages as a construction material and are gaining a lot of ground in the construction sector; the origin of bio-based additives has been used in construction for several centuries. The Ro-

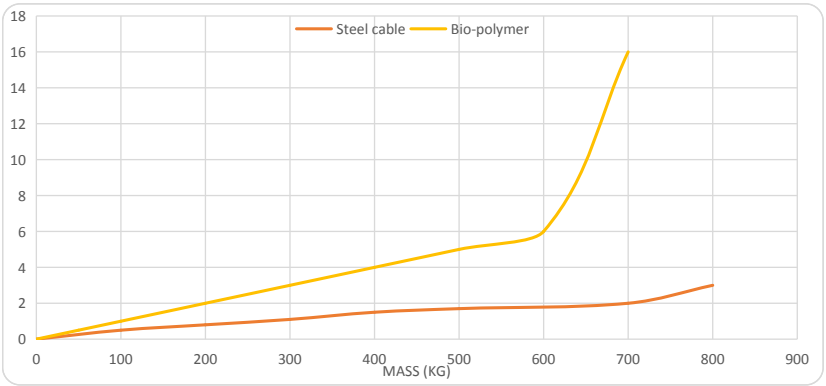

Graph 1. Analysis of strength of the bio-polymer.

mans for several centuries recognized the role of bio mixes to improve construction materials, an example was the use of proteins that served as retarders for plaster. Another great example it's with Vitruvio, that explained that the use of lime mortar could be mixed with vegetable fat to give a better finish to its walls.

This research presents a new construction system based on timber hexagons that are joined sewing joints, through these joints the use of steel and concrete is completely avoided, presenting a great advantage over conventional construction systems. Using the morphological principles of diatoms, we emulate the unions of the hexagons to generate a new lightweight structure of timber. Sewing joints have a great advantage over steel and cement since they connect each panel of hexagons and help to obtain any radius that can be demanded, simply by adjusting the measurements of each hexagon.

3.3 Applying biological principles to form finding

Different studies were carried out prior to the choice of diatoms for the design of the lightweight structure, different types of phytoplankton were analyzed and the aim was to integrate bio-morphological principles into architecture and engineering; therefore, for the form-finding process, it was limited to the geometric principles of diatoms. In the case of the panels, we opted for the *Coscindiscus Radiatus* species due to its hexagonal shape (**Figure 5**), since this geometric shape has great advantages since it allows different connections with the other panels, thus allowing a better distribution of the load.

It is important to highlight that during the last decades, using biology as part of the form-finding process promotes advantages for the design process, since during this process these principles were transferred to different software such as Rhino7, Grasshopper, Karamba and Kiwi. Helping to better develop and optimize this structure. In the case of this structure, it was decided to use parametric design tools that would allow the development of a structure divided into panels and a main structure; the part of the panels forms the main membrane that is supported by 3 wooden beams anchored directly to the floor. As for the measurements in the central part, it is 3.2 meters high and has a maximum length of 8 meters, with a covered area of 50 m^2 (**Figure 6**).

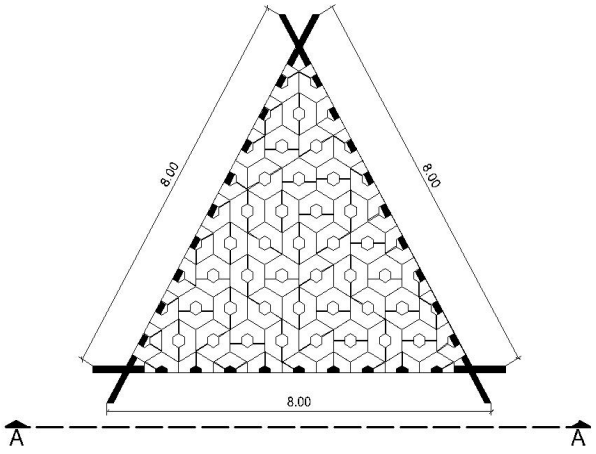

Figure 5. Floor plan of the timber pavilion.

The surface was based on the design of different hexagons that are sandwiched together (one on top of the other) and connected by the biopolymer joints. Different designs were made for the panels and for this structure there were a total of 138 hexagons for the entire surface.

The design of a synclastic structure was chosen, since through the double curvature the shape can be optimized and this is summarized as less material and more covered area. Being a clear example of how to create sustainable and naturally friendly structures. One of the great advantages of this decade is that thanks to technology and digital computing, new opportunities can be developed to develop new geometric shapes that were previously impossible to develop, and this presents great opportunities to develop thanks to form-finding [8]. The development of complex geometric structures and structural optimization are tools of form-finding. Among the innovations of this structure is the link that was obtained from the study of diatoms and how to find the best design for the structure, linking geometry with biology and trying to emulate the principles of biology with the architectural design was a work that helped to develop this structure. This structure integrates a double curvature surface that was developed after several attempts and proposals and this results in an economic structure that also infers not only a lower cost, but also a reduction in energy expenditure and

lower CO_2 contributions to the environment. In particular, the demand for double-curvature surfaces has increased in construction, engineering and architecture since compared to other types of surfaces they present great structural and geometric advantages (**Figure 7**).

4. Conclusions

The present investigation had a result that encompasses different disciplines such as engineering, biology and architecture and is based on the bio-design of the analysis of diatoms and how their geometric shape can optimize a lightweight structure. On the one hand, the bio-morphology of diatoms can have geometric patterns that are a clear example of structures that have patterns that can develop a new construction and adopt forms that optimize. This means that the integration of bio-materials is a clear example of how new construction systems can be used and generate great benefits for the construction sector.

After using parametric design, digital fabrication and structural optimization new possibilities can be developed to make new and complex geometric shapes and this promotes new practices in design that help to obtain better optimization and structural behavior, this translates as a great opportunity to take advantage of these sustainable and economic advantages to apply them to the actual climate crisis.

Thanks to this research and new proposals that are currently being developed in lightweight structures, the progress and advances that this type of structure has been giving new results as they are a clear example of how the construction sector can contribute to climate change; through geometry, materials and structural optimization an efficient form can be developed. When starting this research, we wanted to see how bio-design can be a great tool for the designer and how biological principles can be transmitted to any design. In the case of biological principles, we chose to transfer the geometry to a hexagonal-shaped wooden panel, which was a great innovation to develop new ways of designing. In the end, we conclude that these biological principles can be applied to different types of wood (shape, geometry, connections, structure...) and that through a multidisciplinary vision they can be applied to any structure.

This research promotes a sustainable, innovative and economic design since after different studies and investigations and thanks to biology it was concluded by the use of diatoms due to their geometric and biological principles. It should be highlighted that with this new construction system, biopolymers were used and neither cement nor steel was used for

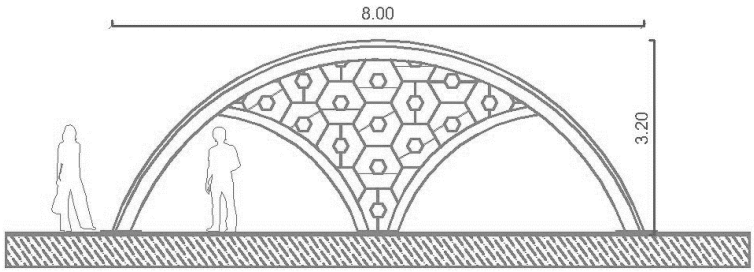

Figure 6. Detail plan of the pavilion.

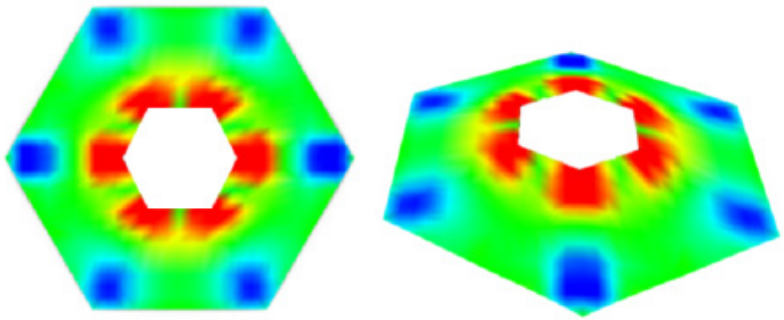

Figure 7. Structural behavior of the panels.

the manufacture and assembly of the structure. Due to the progress in the investigations of the timber structures, it will be possible to obtain better results that benefit the environment and the economy, the development of new construction systems and the integration of new materials into the structures promote sustainable values. This research is a result of the new construction practices and construction techniques that are currently demanded, which benefit architecture and engineering thanks to digital fabrication and architectural design.

Author Contributions

Author 1: Melisa Gálvez Bohórquez (MG)

MG focused on the development of the state of the art and thanks to his experience in the academic world he knew how to land the research questions and the foundations to continue the research. On the other hand, support in the final design of the structure since it has experience in the area of technologies and light structures. through different computer programs I provide the tools to be able to generate a better proposal for the final design as well as the materials that were going to be used.

Author 2: Mauricio Díaz Valdés (MD)

MD was in charge of executing the research stay at the Biology Institute of the National Autonomous University of Mexico, in which he was in charge of analyzing different diatones in order to find the one that best suited the design needs. Thanks to his experience in the field of light structures and his knowledge in digital fabrication and software, the final design of the structure was obtained. In the same way, I carry out the tests within the Engineering Institute of the same university.

Conflict of Interest

There is no conflict of interest.

Acknowledgement

Thanks to the Dr. Hans Martin Ricker of the Institute of Biology of the National Autonomous University of Mexico, for his time and support during this investigation, guiding us in the best way to analyze the different species of *phytoplankton*. Also, to the Faculty of Engineering for supporting us with the machinery and the time to carry out the tests of the joints, as well as indications to be able to optimize the joints and improve the structural behavior of the project.

References

[1] Ellers, O., 1993. A mechanical model of growth in regular sea urchins: Predictions of shape and a developmental morphospace. Proceedings of the Royal Society London. 255(1340), 123-129.

[2] Knippers, J., Menges, A., Bechert, S., 2016. Textile fabrication techniques for timber shells. Advances in Architectural Geometry 2016. vdf Hochschulverlag AG an der ETH Zürich: Switzerland. pp. 154-169.

[3] Thomas, D., 2017. Masters of the structural aesthetic, 1st edition. Springer: Singapore.

[4] Wester, T., 2002. Nature teaching structures. International Journal of Space Structures. 17(2-3), 135-147.

[5] Menges, A., 2009. Performative Wood: Integral Computational Design for Timber Construction [Internet]. Available from: http://papers.cumincad.org/data/works/att/acadia09_66.content.pdf

[6] Schimek, H., Ruffo-Calderon, E., Wiltsche, A. (editors), et al., 2012. Sewing timber panels. An innovative digitally supported joint system for self-supported timber plate structures. Beyond Codes and Pixels: Proceedings of the 17th International Conference on Computer-Aided Architectural Design Research in Asia; Hong Kong. p. 213-222.

[7] Li, J., Knippers, J. (editors), 2015. Pattern and form-their influence on segmental plate shell. Proceedings of IASS Annual Symposia, IASS 2015 Amsterdam Symposium: Future Visions—Timber Spatial Structures; 2015 Aug 20; Amsterdam, Netherlands. USA: International Association for Shell and Spatial Structures (IASS). p. 1-12.

[8] Knippers, J., Menges, A., Gabler, M., et al., 2013. From nature to fabrication: Biomimetic design principles for the production of complex spatial structures. Advances in Architectural Geometry. Spinger: Wien. pp. 107-122.

BILINGUAL PUBLISHING GROUP

Journal of Building Material Science

https://journals.bilpubgroup.com/index.php/jbms

ARTICLE

Experimental Study and Fragility Analysis of Effective-Length Factors in Column Buckling

Brannan Shepherd, Tadeh Zirakian*

Department of Civil Engineering and Construction Management, California State University, Northridge, CA, 91330, USA

ABSTRACT

The design of columns relies heavily on the basis of Leonhard Euler's Theory of Elastic Buckling. However, to increase the accuracy in determining the maximum critical load a column can withstand before buckling, a constant was introduced. This dimensionless coefficient is *K*, also known as the effective-length factor. This constant is often found in building design codes and varies in value depending on the type of column support that is applied. This paper presents experimental and analytical studies on the determination of the effective-length factor in the buckling stability of columns with partially-fixed support conditions. To this end, the accurate *K* value of the columns tested by the Instron Testing Machine (ITM) at California State University, Northridge's (CSUN's) Mechanics Laboratory is determined. The ITM is used in studying the buckling of columns where the supports are neither pinned nor fixed, and the material cross-section rather rests upon the machine while loading is applied axially. Several column specimens were tested and the experimental data were analyzed in order to estimation of the accurate effective-length factor. The calculations from the tested results as well as the conducted probabilistic analysis shed light on how a fragility curve may aid in predicting the effective-length value of future tests.

Keywords: Column buckling; Fragility curve; Critical loading; Effective length factor; Fixity

1. Introduction

Column buckling can be defined as the abrupt lateral displacement of a column under which maximum loading is applied. This occurs mainly in members with a high slenderness ratio, meaning the length of the member is much greater than the width

*CORRESPONDING AUTHOR:

Tadeh Zirakian, Department of Civil Engineering and Construction Management, California State University, Northridge, CA, 91330, USA; Email: tadeh.zirakian@csun.edu

ARTICLE INFO

Received: 30 January 2023 | Revised: 5 March 2023 | Accepted: 13 March 2023 | Published Online: 20 March 2023

DOI: https://doi.org/10.30564/jbms.v5i1.5432

CITATION

Shepherd, B., Zirakian, T., 2023. Experimental Study and Fragility Analysis of Effective-Length Factors in Column Buckling. Journal of Building Material Science. 5(1): 9-16. DOI: https://doi.org/10.30564/jbms.v5i1.5432

of the cross-section. Shorter-length members will not experience buckling but rather crushing under greater loads. Regardless, critical loads for columns of any slenderness ratio can be calculated. Leonhard Euler's Theory for Elastic Buckling produced such an equation which is as follows:

$$P_{cr} = \frac{\pi^2 EI}{(l/r)^2} \quad (1)$$

where E is the modulus of elasticity of the material being used, l is the length of the member, and r is the radius of gyration, which is equivalent to:

$$r = \sqrt{\frac{I}{A}} \quad (2)$$

Here, I is seen as the bending moment of inertia and A is the cross-sectional area of the member. With Equation (1), values obtained for various columns with differing support connections yield unreliable results. By substituting in the effective-length constant "K" of the column being analyzed, the equation then converts to:

$$P_{cr} = \frac{\pi^2 EI}{(Kl)^2} \quad (3)$$

This then provides more accurate critical load results theoretically as well as for physical applications [1]. Specific K values are to be used when calculating critical loads with different column support connections. For example, columns that have fixed connections on both ends will utilize a K value of 0.5, and columns with simply supported pinned connections will use a K value of 1. The goals established before conducting any experimentation were to calculate an accurate K value for the supporting connections on California State University, Northridge's (CSUN) Instron Testing Machine (ITM), since it will be used for this case study specifically, and undergo probabilistic analysis of results. This is achieved by creating a fragility curve that aids in predicting the probability of K values that would be produced in future tests.

2. Literature review

The primary focus of this case study is on the effective length constant for columns, however, there are far more variables that can change the overall effective length of a column. Hibbeler defines the effective length of a column as the distance between points of zero moments [1,2]. Therefore, supports that limit rotation will provide a moment reaction and produce an internal inflection point. This is the case with completely fixed supports. A moment reaction at both the top and bottom of the member decrease the effective length resulting in an effective length factor of K = 0.5. For pinned supports, there are no moment reactions at the end conditions therefore, the effective length results in the full length of the member since the closest values of zero moments are at the connections. An experimental example of this can be cited by Bouras et al. [3]. The experimental design utilizes a notched cylinder that accepts the column, and a welded angle with a Teflon sheet that guides the cylinder in rotation emulating a pinned connection. With this setup, the effective length factor used is K = 1.0 since the resulting zero moments will lie at the connections.

As previously stated, not only is the support condition the only variable that plays a role in the overall effective length. Referring to Tian et al. [4], columns can contain various stiffnesses, cross-sectional areas, distributions in axial loading, and differing ratios between lengths. These variables may only take effect when considering stepped columns composed of materials other than wood elements. However, the theory and determination of critical load behaviors still extend from the foundational Elastic Buckling Theory. Expanding on the notion that many studies in modern engineering stem from Euler's Theory, in Falborski et al.'s study of column base fixity [5], the base support of a column within a frame can be manipulated to obtain a certain degree of flexibility. With this flexibility, the inflection points of the member can be adjusted to lessen the amount of internal moment received at the upper end of the column where the structure is more vulnerable, and result in an increase in the moment at the base where the foundation can resist greater moment reactions. This enables the structure to withstand higher amounts of lateral loadings, such as wind or earthquakes, all while under uniform axial loading.

In any study involving structural behavior under

extreme loading, the allowable stress and strain of material are vital. In Euler's Theory, the modulus of elasticity is the primary component relating stress and strain considering the modulus under axial loading is the quotient of normal stress and strain. Avallone et al. [6] display these relations many times using stress-strain curves. When members are placed under increasing axial loading, the elements' material properties of stress and strain demonstrate a linear-proportional relationship which is called the elastic range. Outside this range lies other circumstances with vibrational forces and accelerations that will not be covered in this experiment but still are immensely important when pertaining to structural designs in earthquake engineering.

In the analysis of earthquake effects on structures, seismic fragility curves have been explored with the goal of determining the vulnerability of structures if induced by such type of lateral loading. In this paper, the basic use of fragility curves will be explored in determining the probability of effective length constants however, studies such as one under Rajeev and Tesfamariam [7] reveal more in-depth uses of this tool. In their study, they analyze multiple building failures due to earthquakes and compile several variables such as a number of weak stories, year of construction, beam-column connections, and the topology of the site. With these factors applied they can create relations between the demand of the earthquake in question and the structural capacity of the building to make predictions on other buildings similar in design and determine its probability of survival or failure with an earthquake of similar magnitude. Guevara-Perez [8] also discusses the importance of beam-column connections in the result of weak stories that are a major factor in the ability of a structure to successfully endure an earthquake.

Many factors play a role in the behavior of columns and through a review of various studies involving advanced concepts in engineering we can see that at the foundation level, column buckling shows there are key differences in behavior when something as simple as a support condition is altered. With this alteration, the behavior of columns will ultimately create effects higher up the chain in structural analysis. By establishing a better understanding of how effective length factors and fragility curves function with a single member, made of wood in this case, the more advanced theories and concepts may begin to see effects as well within larger systems, structures, and materials. They branch off from the basic understanding of column buckling and its reactions to compressive loading.

3. Experimental design

The support connections for the ITM are neither fully fixed nor pinned, therefore, the end connections will be referred to from here on out as partially fixed. For example, as seen in **Figures 1 and 2**, the cross-section of the member is rested flush to the crossheads of the machine, which only partially limits rotational and translational displacements. **Figure 3** shows how the test specimen is positioned in ITM. 15 Douglas Fir specimens roughly 35 inches in length were prepared to undergo compression in the partially fixed machine connections. Calculations such as weight, volume, density, cross-sectional area, slenderness ratio, and moment of inertia were then taken for each sample as shown in **Table 1**. For this experiment, a Modulus of Elasticity (E) of 1.95×10^6 psi is established considering this is the same value dedicated to the wood used in CSUN's laboratory for other experiments. This also maintains the accuracy of results in relation to past and future tests conducted at CSUN. Each specimen was then carefully positioned in the ITM crosshead and testing was conducted through the program TestWorks QTEST. Information about the specimen being tested such as length and cross-sectional area was input into the program and then, at a rate of 0.01 in/min, the crossheads of the ITM compressed the specimens axially until buckling or complete failure occurred. QTEST then provided peak stress (σ_{cr}) and critical load (P_{cr}) values from each sample tested. The details of the ITM as well as the length and cross-section dimensions of a typical test specimen are illustrated in **Figure 4**.

Figure 1. Top crosshead connection.

Figure 2. Bottom crosshead connection.

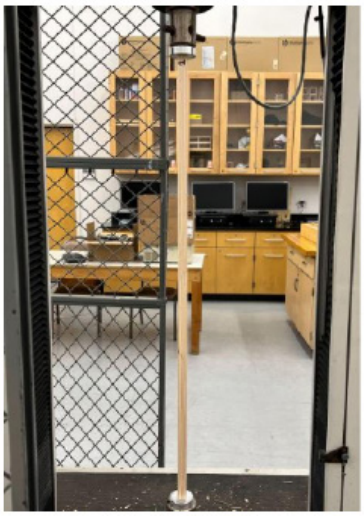

Figure 3. Specimen placed in ITM.

Table 1. Properties of the test specimens.

Wood specimen	Length (in)	Greatest ccsross section dimension (Dmax, in)	Least cross section dimension (Dmin, in)	Cross section area (in^2)	Weight (oz)	Volume (in^3)	Density (oz/in^3)	Slenderness ratio (Min)	Slenderness ratio (Max)	Moment of inertia (in^4)
1	35.000	0.727	0.693	0.504	6.30	17.633	0.357	50.505	48.143	0.0202
2	35.063	0.729	0.716	0.522	5.30	18.301	0.290	48.970	48.097	0.0223
3	35.000	0.734	0.726	0.533	6.70	18.651	0.359	48.209	47.684	0.0234
4	35.063	0.719	0.712	0.512	5.50	17.949	0.306	49.245	48.766	0.0216
5	35.000	0.721	0.714	0.515	5.30	18.018	0.294	49.020	48.544	0.0219
6	35.000	0.724	0.718	0.520	6.70	18.194	0.368	48.747	48.343	0.0223
7	35.000	0.728	0.717	0.522	6.50	18.269	0.356	48.815	48.077	0.0224
8	35.063	0.727	0.715	0.520	6.30	18.226	0.346	49.038	48.229	0.0221
9	35.063	0.717	0.709	0.508	5.40	17.824	0.303	49.453	48.902	0.0213
10	35.000	0.729	0.718	0.523	6.90	18.320	0.377	48.747	48.011	0.0225
11	35.063	0.729	0.725	0.529	6.30	18.531	0.340	48.362	48.097	0.0232
12	35.000	0.733	0.728	0.534	6.50	18.677	0.348	48.077	47.749	0.0236
13	35.063	0.733	0.716	0.525	5.50	18.402	0.299	48.970	47.834	0.0224
14	35.063	0.719	0.727	0.523	5.40	18.328	0.295	48.229	48.766	0.0230
15	35.000	0.738	0.728	0.537	6.90	18.804	0.367	48.077	47.425	0.0237

4. Evaluation of experimental results

After a certain amount of compression, each column either buckled or completely failed to result in fractures, as shown in respective **Figures 5 and 6**. Some members that were not fractured from testing remained in the elastic range and reverted to their original linear state after loading was removed. However, there was slight deformation left over and a bend in the specimen could be seen. All data obtained from the testing machine was placed into tabular form and comparisons were made between the experimental and theoretical critical load based on support connections, which can be seen in **Table 2**. Average experimental values for peak stress and critical load were 2,278.69 psi and 1,188.77 lbs, respectively. We can assume that variations in both values are due to the inhomogeneity of the wood

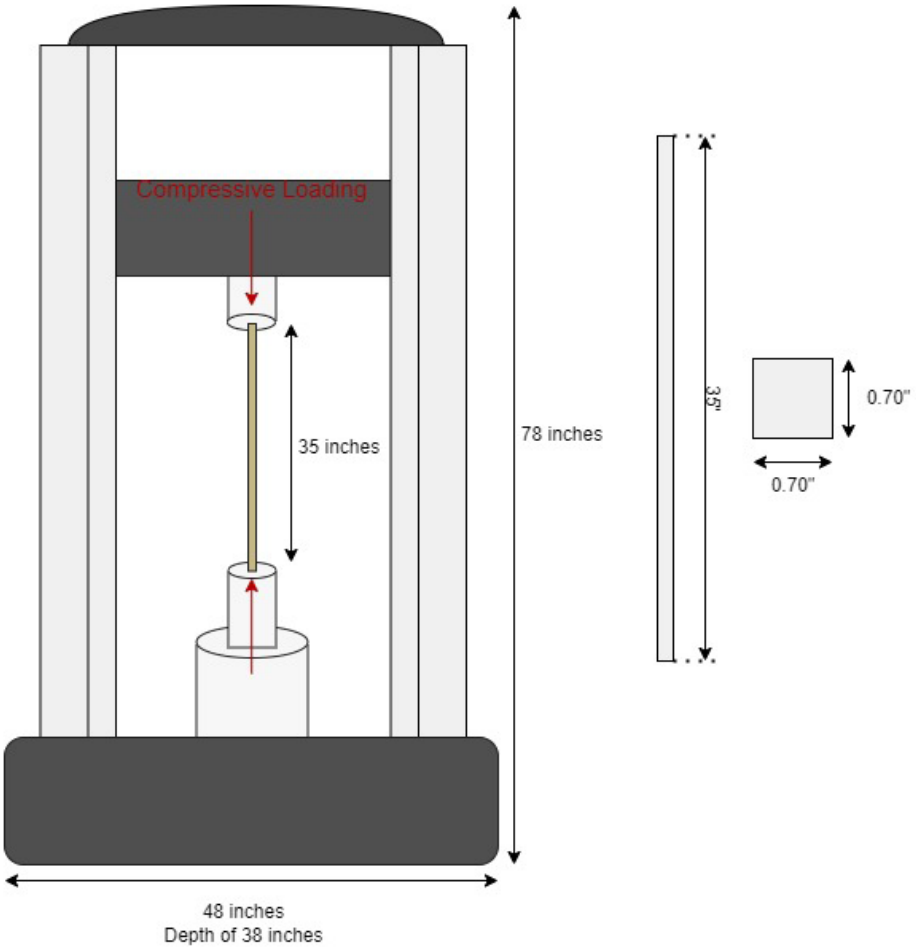

Figure 4. Details of the ITM and geometrical dimensions of a typical test specimen.

Figure 5. Specimen #6 buckling under compression.

Figure 6. Specimen #3 ruptured after compression.

Table 2. Summary of theoretical calculations and test data.

Wood specimen	Fixity (%)	Theoretical P_{cr} (SS)	Theoretical P_{cr} (FF)	Experimental P_{cr} (PF)	Peak stress (psi)	Experimental effective length factor (*K*)	Normal distribution
1	77.115	316.775	1,267.101	839.10	1,665.60	0.614	0.962
2	90.104	349.087	1,396.349	1,156.20	2,245.10	0.549	0.521
3	91.834	367.725	1,470.899	1,257.20	2,359.30	0.541	0.429
4	89.931	338.560	1,354.242	1,117.80	2,183.60	0.550	0.530
5	75.990	343.595	1,374.380	893.70	1,736.00	0.620	0.973
6	93.781	350.856	1,403.424	1,243.90	2,393.00	0.531	0.331
7	101.037	351.322	1,405.290	1,434.90	2,749.00	0.495	0.081
8	92.223	346.673	1,386.692	1,193.80	2,296.60	0.539	0.409
9	97.101	333.369	1,333.476	1,259.40	2,477.50	0.514	0.190
10	98.631	353.279	1,413.116	1,375.20	2,627.30	0.507	0.140
11	79.898	362.417	1,449.669	1,005.00	1,901.60	0.601	0.920
12	84.400	370.267	1,481.068	1,108.30	2,076.90	0.578	0.791
13	96.486	351.003	1,404.011	1,310.30	2,496.60	0.518	0.213
14	92.249	360.412	1,441.649	1,241.70	2,375.50	0.539	0.408
15	96.614	372.793	1,491.171	1,395.10	2,596.70	0.517	0.208
Average	90.493	351.209	1,404.836	1,188.77	2,278.69	0.548	
					Std. Dev.	0.038	

members themselves. Some members had less or greater densities as well as internal defects, seen in most wooden materials. For example, a material such as steel or any other metal alloy is pure and homogeneous throughout the entire length of the member, whereas wood may have internal knots in the wood or initial fractures that may not be seen on the surface. Since we were given the experimental P_{cr}, the experimental *K*-value for each specimen was calculated and an average effective length constant of 0.548 was found. Effective length constants from each member can be seen in **Table 2**. **Figure 7** allows a visual representation of the variability in effective length values. Clear observations were made for the tested columns and a general effective length ratio lies somewhere between 0.5 and 0.6.

Using Equation (3), theoretical critical loads with fixed and pinned connections were calculated and the results show that the experimental critical load lies in-between fixed and pinned connections but resembles fixed circumstances more. This is due to the previously stated fact that the partially fixed crossheads of the ITM do not completely limit rotation, so the columns are able to, just slightly, have an increased effective length. **Figure 8** shows this slight rotational freedom when subjected to the compressive load. To further analyze the degree to which the partially fixed supports constrain rotations and translations, its fixity percentage was calculated.

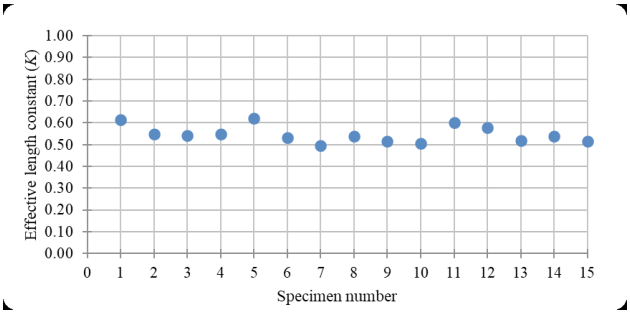

Figure 7. Effective length constants of test specimens.

Figure 8. Upper crosshead support under loading.

5. Probabilistic analysis

Columns contain a certain level of fixity in the supports. What influences this level of fixity is the degrees of freedom allowed in the support condition. For example, a fixed-end condition restricts translation in the *x*, *y*, and *z* directions as well as rotation therefore it contains fixity in all six degrees of freedom. To further analyze the behavior of columns placed in the ITM, calculations of fixity percentage were obtained. Taking the average *K*-value of 0.548 from the experimental data, interpolations between the fixed and pinned supports were made. The equation to determine this value is as follows:

$$\frac{0.548-0.50}{1-0.50} = \frac{X_n-100}{0-100}$$
$$X_n = \left[-\left(\frac{0.548-0.50}{0.50}\right)\cdot 100\right] + 100 \quad (4)$$

Allowing fixed supports to have 100 percent fixity and a *K*-value of 0.50, pin-supported conditions having zero percent fixity and a *K*-value of 1.0, interpolation between the two conditions concluded that the columns tested under partially fixed obtained an average fixity percentage of 90.49 percent. All values for individual members can be seen in **Table 2**. Again, this supports the observation that a partially fixed support such as the one seen in CSUN's ITM lies closer in relation to fixed-end conditions than simply supported, but still results in displaying its own distinct column behavior.

Further probabilistic analysis was done through the generation of a fragility curve. Fragility curves are S-shape plots primarily used in earthquake engineering to assess the damage state of structures or to aid in the prediction of how much damage a structure will encounter when earthquake conditions are applied. This is done through a cumulative probability distribution plotted with earthquake intensity and damage grades. This method of analysis can also be applied to column buckling. To do this, the mean and standard deviation of the effective length values from the entire column set is applied to a cumulative distribution function. These values can also be seen in **Table 2**. Then, the probability distribution was plotted against the original respective *K*-values obtained from experimental testing. The plot is shown in **Figure 9**.

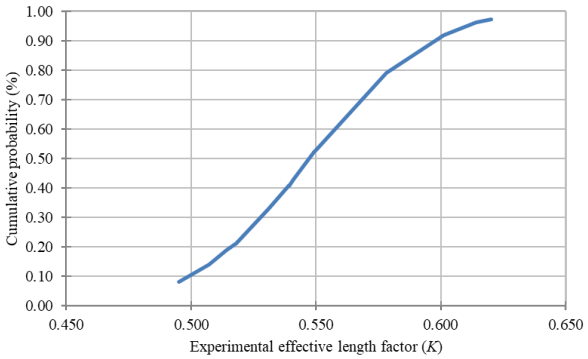

Figure 9. Fragility curve.

Along the ordinate, we can see the range is from zero to one. This is the probability percentage that a given effective length value will show. In other words, by taking any reference point along the curve the area underneath the curve represents the probability that the respective effective length ratio will occur. For example, at the effective length value of 0.55 the cumulative probability outputs a value of about 53 percent. This means that for future testing of these columns, there is a 53 percent probability that the resulting effective lengths between 0.495 and 0.55 will be produced. The same analysis is done from the higher and lower ends of the curve. At the effective length reference point of 0.6 the corresponding probability is around 10 percent that a greater effective length factor is produced and at an effective length factor of 0.5 the probability is less

than 10 percent to produce a value less than or equal to 0.5. This coincides with the behavior of the columns and concludes that through further testing, 80 percent of columns will produce an effective length between 0.5 and 0.6 with a larger majority resulting closer to 0.55.

6. Conclusions

In this paper, the determination of the effective-length factors of columns with partially-fixed end supports and subjected to axial loading was investigated through the adoption of experimental and analytical approaches. To this end, a case study on the testing of columns by CSUN's ITM was conducted and discussed. The support conditions of CSUN's ITM allow the columns to produce an alternate behavior due to external compression that is not seen under traditional support connections such as fixed and pinned conditions. A partially-fixed connection with an average effective length of about 0.55, although not far from fixed conditions, still reveals there is slightly different behavior and is significant enough to be classified as its own support condition. Creating a fragility curve of the column behavior also provided a predictability tool to determine how the column will behave under future testing. The effectiveness of the adopted experimental, analytical, and probabilistic approaches in the determination of the accurate effective-length factor in columns with partially-fixed supports was demonstrated in this research endeavor. In particular, the application of the fragility methodology in efficient buckling stability assessment of structures seems to be quite promising.

Conflict of Interest

There is no conflict of interest.

Acknowledgement

The authors would like to express their great appreciation for funding made possible in support of this research endeavor through the CSU-LSAMP (California State University Louis Stokes Alliance for Minority Participation) program via the NSF (National Science Foundation) grant #HRD-1302873 and the Chancellor's Office of the California State University.

References

[1] Hibbeler, R.C., 2023. Mechanics of materials (9th edition). Upper Saddle River: Prentice Hall.

[2] Crandall, S.H., Dahl, N.C., Lardner, T.J., et al., 2012. An introduction to the mechanics of solids (3rd Edition). McGraw Hill: New York.

[3] Bouras, F., Chaplain, M., Nafa, Z., 2010. Experimental and modelling buckling of wood-based columns under repeated loading. EPJ Web of Conferences. 6, 28003.
DOI: https://doi.org/10.1051/epjconf/20100628003

[4] Tian, W., Sun, J., Hao, J., 2021. Effective length factors of three- and two-segment stepped columns. Journal of Constructional Steel Research. 181, 106585.
DOI: https://doi.org/10.1016/j.jcsr.2021.106585

[5] Falborski, T., Hassan, A.S., Kanvinde, A.M., et al., 2020. Column base fixity in steel moment frames: Observations from instrumented buildings. Journal of Constructional Steel Research. 168, 105993.

[6] Avallone, E., Baumeister, T., Sadegh, A., 2006. Marks' standard handbook for mechanical engineers (11th Edition). McGraw Hill: New York.

[7] Rajeev, P., Tesfamariam, S., 2012. Seismic fragilities for reinforced concrete buildings with consideration of irregularities. Structural Safety. 39, 1-13.
DOI: https://doi.org/10.1016/j.strusafe.2012.06.001

[8] Guevara-Perez, T., 2012. "Story" and "Weak Story" in Earthquake Design: A Multidisciplinary Approach. Indian Institute of Technology Kanpur [INternet]. Available from: https://www.iitk.ac.in/nicee/wcee/article/WCEE2012_0183.pdf

BILINGUAL PUBLISHING GROUP

Journal of Building Material Science

https://journals.bilpubgroup.com/index.php/jbms

EDITORIAL

Challenges and Trends for Multifunctional Materials

Ying Huang**, *Xingyu Wang

North Dakota State University, Fargo, ND 58078, USA

1. Background

Materials science is the study of materials, their properties and their applications. As the rapid development of material science, materials tend to approach multifunctionality. Multifunctional materials are designed to perform multiple responsibilities through prudent combinations of different functional capabilities. Typically, each function contributes a distinct physical or chemical process that can deliver system-level improvements beyond the status quo. Even though some researchers have defined "smart material" as multifunctional materials (MFM), multifunctional composites (MFC), multifunctional structures (MFS), and multifunctional material systems (MFMS), the term "multifunctional materials" will be used to refer to all of these materials, composites, and structures in this paper [1]. One of the main advantages of multifunctional materials is their capacity to simultaneously accomplish multiple functions, which can decrease the need for various materials and components in the system. This benefit can result in reduced weight, higher efficiency, and superior properties and the development of multifunctional materials enables technologies that were previously impossible. The properties of multifunctional materials could vary substantially based on the applications and demands of the material. For example, the materials may respond to heat (thermal), stress & strain (mechanical), electrical, magnetic, pH, moisture, light (photonic), and molecular or biomolecular substances, and others. By incorporating these materials into composites, numerous functionality, including self-healing, self-sensing, self-cleaning, electric conductive, thermal conductive, membrane, shape memory, and actuation, can be achieved. Therefore, multifunctional materials can improve processes and products, create several avenues to increase sustain-

*CORRESPONDING AUTHOR:
Ying Huang, North Dakota State University, Fargo, ND 58078, USA; Email: ying.huang@ndsu.edu

ARTICLE INFO
Received: 9 March 2023 | Accepted: 14 March 2023 | Published Online: 21 March 2023
DOI: https://doi.org/10.30564/jbms.v5i1.5521

CITATION
Huang, Y., Wang, X.Y., 2023. Challenges and Trends for Multifunctional Materials. Journal of Building Material Science. 5(1): 17-19. DOI: https://doi.org/10.30564/jbms.v5i1.5521

ability, and have a direct and positive impact on economic growth, environment, and quality of life.

2. Challenges

To unlock the full potential of multifunctional materials, several challenges need to be addressed. These challenges include the needs for 1) multi-disciplinary collaboration, 2) a suitable balance of the different properties of the material, 3) development of environmentally sustainable materials, 4) cost-effective manufacturing and implementation methods, and 5) high durability of the materials to enable them to withstand environmental conditions and allow them to be used in real-world applications. The first major challenge in developing multifunctional materials is the requirement for multi-disciplinary approaches. The key to the success of multifunctional materials is the integration of various properties into a single material, which involves knowledge of materials science, physics, chemistry, and engineering. This challenge creates difficulties in terms of collaboration and communication among experts from several scientific fields. Secondly, the ideal development of multifunctional materials can only be accomplished by combining multiple properties without sacrificing any of them. Until now, optimizing multi-functions often require a trade-off between them, and achieving the right balance can be challenging. In addition, manufacturing multifunctional materials might be complicated and require specific equipment and experience. Frequently, the manufacturing of multifunctional materials includes complicated and time-consuming procedures that demand high precision and control and this can raise manufacturing expenses and restrict application to large-scale usage. Finally, the performance of multifunctional materials can be affected by environmental factors such as mechanical damage, chemical exposure, temperature, humidity, UV irradiation, and others; therefore, developing materials that can survive these environments is a major challenge.

3. Trends

Despite the challenges stated previously, the development of multifunctional materials is an attractive field of study, motivated by the potential to develop novel products that can meet the diverse demands of society. Future trends in this subject include the invention of environmentally sustainable materials that can be manufactured using sustainable processes. As the world progressively focuses on sustainability and lowering carbon emissions, future research on multifunctional materials will need to address the environmental impact. This research strategy involves the use of biodegradable materials, materials derived from renewable sources, and recyclable or reusable materials. This also brings the demands of developing multifunctional materials that can address specific sustainability challenges, such as air/water purification or green energy generation.

All cutting-edge technologies and materials will eventually be evolved through more efficient and cost-effective procedures, enabling them to be widely implemented in civil society and improving how people live and work. Even though the area of multifunctional materials is still in its beginnings, the ultimate goal is to develop materials with practical applications. Hence, continuous research about how multifunctional materials could be incorporated into real-world systems, such as electronics, aerospace engineering, and healthcare devices, will be essential for promoting innovation and generating new markets [2]. Moreover, future civil engineering structures will undoubtedly integrate and consist of multifunctional materials. Aside from the attractive functions and properties such as self-monitoring, self-healing, high UV and chemical resistance, color-changing, temperature regulation, air-cleaning, and energy harvesting, it is anticipated that multifunctional materials with properties such as sustainability, cost-savings, and enhanced durability will have the potential to be utilized on a global scale.

Conflict of Interest

There is no conflict of interest.

References

[1] Ferreira, A.D.B., Nóvoa, P.R., Marques, A.T., 2016. Multifunctional material systems: A state-of-the-art review. Composite Structures. 151, 3-35.

[2] Lendlein, A., Trask, R.S., 2018. Multifunctional materials: Concepts, function-structure relationships, knowledge-based design, translational materials research. Multifunctional Materials. 1, 010201.

BILINGUAL PUBLISHING GROUP

Journal of Building Material Science

https://journals.bilpubgroup.com/index.php/jbms

ARTICLE

Effects of Curing Methods on the Permeability and Mechanism of Cover Concrete

Wang Hao[1], Baolin Guo[2,3], Yongzhi Guo[3], Ruishuang Jiang[3], Fangli Zhao[2*], Baomin Wang[2*]

[1] *Shandong Hi-speed Company Limited, Jinan, Shandong, 250101, China*

[2] *School of Civil Engineering Dalian University of Technology, Dalian, Liaoning, 116000, China*

[3] *Transportation Research Institute of Shandong Province, Jinan, Shandong, 250100,China*

ABSTRACT

Curing methods are one of the most important factors in determining the quality and compactness of cover concrete. The effect of curing methods on the water absorption and sorptivity coefficient of cover concrete with the substitution ratio of fly ash (FA) and ground granulated blast slag (GGBS) for cement between 30 wt% and 40 wt% was studied by capillary water absorption test. The vacuum saturation test and mercury intrusion test were employed to characterize these differences in the pore structure of cover concrete under different curing methods. With further analysis of the compactness of microstructure by SEM, the mechanism of the impact of curing methods on the permeability of cover concrete was revealed. The results obtained indicate that the effect of curing methods on the water absorption, sorptivity coefficient and porosity of cover concrete shows the trend of natural curing > cover curing > water curing > standard curing. It is also shown that reasonable curing is advantageous to reduce the porosity and permeability of cover concrete. In natural curing conditions, the appearance of porosity increasing and pore structure coarsening is more critical for covering concrete with mineral admixtures than for pure cement concrete. Therefore, the permeability of cover concrete with mineral admixtures is more sensitive to the early-age curing methods.

Keywords: Curing methods; Cover concrete; Permeability; Capillary water absorption; Porosity

*CORRESPONDING AUTHOR:

Fangli Zhao, School of Civil Engineering Dalian University of Technology, Dalian, Liaoning, 116000, China; Email: zhaofl1996@163.com;
Baomin Wang, School of Civil Engineering Dalian University of Technology, Dalian, Liaoning, 116000, China; Email: wangbm@dlut.edu.cn

ARTICLE INFO

Received: 20 February 2023 | Revised: 20 March 2023 | Accepted: 27 March 2023 | Published Online: 30 March 2023
DOI: https://doi.org/10.30564/jbms.v5i1.5484

CITATION

Hao, W., Guo, B.L., Guo, Y.Zh., et al., 2023. Effects of Curing Methods on the Permeability and Mechanism of Cover Concrete. Journal of Building Material Science. 5(1): 20-31. DOI: https://doi.org/10.30564/jbms.v5i1.5484

1. Introduction

Concrete curing is defined as the process of concrete conducting adequate hydration and continuous hardening by providing a suitable temperature and moisture [1]. Wet curing is critical to both strength and durability of concrete [2], but the strength of concrete has not grown alongside durability. The test results obtained by Dinku and Reinhardt [3] showed that the sorptivity coefficient has a very good relevance to gas permeability.

The permeability is widely used as an index for the durability characterization of concrete, and is mainly affected by the combination of curing methods and mineral admixtures [4]. The application results show that the chloride-resistant permeability, carbonizing-resistant capability and freezing-resistant property of wet-cured concrete are superior to that of dry-cured concrete [5-7]. Liu indicated that the gas permeability of the mixtures prepared by replacing cement with 0%-50% by weight of slag is lower than pure cement mixtures [8]. Basheer and Nolan [9] reported that the moisture distribution within 30 mm of the concrete surface is highly susceptible to environmental changes. With premature exposure to wind and sun, the moisture contained in the cover concrete will evaporate rapidly, forming interconnected capillary channels, which reduces the impermeability of concrete [10]. Additionally, the interconnected pores and micro-cracks of cover concrete provide passage for moisture and corrosive media into the internal concrete, which is the chief cause of concrete cracks and steel corrosion [11,12].

Recent research on early-age curing regimes mainly focuses on the effects of curing method, curing temperature and curing humidity on the mechanical and durability of concrete [2,13-15]. Jiang [16] studied the effect of early-age curing temperature and thermal insulation on the 28 d compressive strength and microscopic properties of ultrahigh performance concrete (UHPC), the results have shown that the compressive strength and matrix density increase due to early curing temperature increment, and the thermal insulation curing could be used instead of the steam curing [17]. It has been observed that the early strength of concrete increases significantly with the curing temperature [18,19]. It has been verified by some researchers that heat damage from steam curing has a disadvantageous influence on the durability evaluation of concrete [20,21]. Bai [22] investigated the linkage between capillary water absorption, strength and carbonization depth of composite cementitious concrete under dry curing and water curing conditions. It can be seen that the capillary water absorption and carbonization depth of dry-cured concrete increased and the strength decreased in comparison with concrete under water curing [23]. But this difference between the dry curing and water curing decreased with the metakaolin content, and increased with the fly ash content [24]. Capillary water absorption is able to characterize the ease of porous materials to transfer water through capillaries. Considering results showed of capillary transport of water as a function of curing methods, water-binder ratio and composition of materials, water absorption is correlated with the pores on concrete, especially for cover concrete [25,26]. Khatib and Mangat [27] reported the differences in water absorption of the concrete between the surface and the interior, and the results have shown that the water absorption of the top of the concrete cube is several times greater than that of the inside [28]. Nevertheless, the study of quantitative characterization of the effects of curing methods on the water absorption and the pore distribution of cover concrete has been reported rarely.

Against the above background, the study is dedicated to exploring and characterizing the effects of curing methods on the permeability of cover concrete with high-volume mineral admixture. Four curing methods including natural curing, cover curing, standard curing and water curing (various humidity conditions) and four mixtures (different cementing materials systems) were designed in this research. Water absorption and sorptivity coefficient measured by the capillary water absorption test were applied to quantitatively characterize the effect of curing methods on the permeability of cover concrete. Meanwhile, simultaneous total porosity and pore structure were analyzed to investigate how both can affect the

permeability of cover concrete. Moreover, to further mechanism study, the thermo-gravimetric analysis (TGA) and scanning electron microscopy (SEM) were adopted to describe the hydration degree and microstructure of cover concrete. This plays an important role in providing data support for the durability evaluation of cover concrete prepared by highly adding a number of mineral admixtures.

2. Experimental programme

2.1 Raw materials and mix ratio

The cement used in this study is P·O 42.5 grade ordinary Portland cement (OPC) obtained from Shan Dong Wanhua Chemical Group Co., Ltd, China. The density of cement is about 3.15 g/cm^3, and its specific surface area is 3370 cm^2/g. **Table 1** gives cement's physical properties. The fly ash (FA) of class I and ground granulated blast slag (GGBS) of grade S95 were used as replacement materials. The density and specific surface area of FA are 2.25 g/cm^3 and 3800 cm^2/g, and that of GGBS is 2.89 g/cm^3 and 4400 cm^2/g. **Table 2** presents the chemical components of cement and mineral admixtures. Fine aggregate (S) is ISO Standard Sand that complied with ISO 679 Standard.

Four mixtures containing pure cement (marked as OPC), fly ash (30% by mass of cementitious materials, marked as FA 30), ground granulated blast slag (40% by mass of cementitious materials, marked as S40), and a combination of fly ash and slag (15% and 20% by mass of cementitious materials respectively, marked as FA15S20) were evaluated in the study. **Table 3** presents the detailed proportions of four different mixtures. The binder-to-sand ratio (B/S) in all mixtures was the same and fixed at 0.5. As shown in **Table 3**, water-binder mass ratios (W/B) of 0.35 and 0.45 were designed for each mixture.

2.2 Sample preparation and curing

According to the predesignated mix ratio, the fresh mixture was prepared and then cast into wood molds with dimensions of 200 mm × 200 mm × 20 mm. The mold is made of wood plywood. The moisture and continuous casting do not affect the mold quality. After compacting, the slab samples were cured till the test timing of 7 days. Thanks to the addition of mineral admixture and relatively low water binder ratio, reduced bleeding tendency was presented. Immediately after demolding, the slab

Table 1. Basic properties of cement.

Standard consistency water consumption	Setting time (min)		Fineness (%)	Soundness	Flexural strength (MPa)		Compressive strength (MPa)	
(%)	Initial setting	Final setting	80 μm		3 d	28 d	3 d	28 d
28.4	205	260	0.5	Qualified	4.8	6.8	22.6	44.8

Table 2. Chemical composition of binders.

Material	CaO	SiO_2	Al_2O_3	Fe_2O_3	K_2O	SO_3	Na_2O	MgO
Cement	60.00	23.20	6.90	2.58	0.88	3.97	0.28	1.74
Fly ash	2.71	47.20	37.62	4.55	1.15	2.06	0.49	2.59
Slag	39.59	33.89	14.22	0.91	0.64	2.96	0.36	6.43

Table 3. The mixture proportion design.

Mix code	W/B	Cement (kg/m^3)	Fly ash (kg/m^3)	GGBS (kg/m^3)	Sand (kg/m^3)	Water (kg/m^3)
OPC	0.35 or 0.45	2636	0	0	5273	923
FA30		1845	791	0	5273	923
S40		1582	0	1054	5273	923
FA15S20		1714	395	527	5273	923

specimens from every mixture were subjected to the following four typical curing methods: (i) Natural curing (lack of moisture curing, samples were placed outside at the average temperature of 26.7 °C and the average relative humidity of 60%); (ii) cover curing (samples were sealed with plastic film to prevent moisture evaporation and placed indoors at the average temperature of 20 °C); (iii) standard curing (samples were cured in a curing room with the temperature at 20 ± 2 °C and relative humidity at 98%); (iv) water curing (the samples were demolded and then performed in a water tank filled tap water at the temperature of 20 °C).

2.3 Experimental methods

Capillary water absorption test

The quality of curing has a direct impact on the permeability of covered concrete. The specimens with a dimension of 200 mm × 200 mm × 20 mm were employed to simulate the surface of concrete for the test of capillary water absorption and characterization of permeability. According to ASTM C 1585-04 [29], the capillary water absorption test was carried out as shown in **Figure 1**. At first, the samples of the specified age were dried at 105 °C until constant weight. Then, the lower surface of 200 mm × 200 mm of samples was contacted with water, and the bottom of the sample was exposed to water at approximately 3 mm, to keep a constant height of water level. Meanwhile, the mass of the specimens was recorded every 5 min during the initial process of water absorption, and later recorded every 30 min for 1660 min.

The water absorption I and sorptivity coefficient S were calculated as:

$$I = \frac{(i_t - i_1)}{\rho_w A} = S\sqrt{t} \quad (1)$$

where I is water absorption, mm; $(i_t - i_1)$ is the mass of water adsorbed in, g; ρ_w is the density of water, and the value is 0.001 g/mm^3; A is the cross-section of the sample exposed to water, mm^2; S is a sorptivity coefficient, mm/min$^{0.5}$; t is time, min.

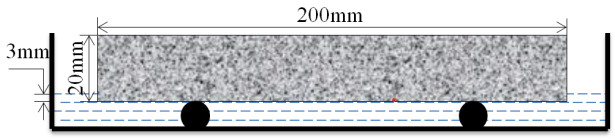

Figure 1. Schematic diagram of capillary water absorption test.

Vacuum saturation test

After measuring the water absorption, the vacuum saturation test was adopted immediately to determine the total porosity of cover concrete. Due to the significant impact of curing methods on the porosity of cover concrete [30], the plate-type specimen was directly used for testing to better characterize the actual structure. The specimens conducted vacuum accelerated saturated water and marked the mass of the specimen after vacuum water saturation as m_s. Then, the specimens were dried at 105 °C for 12 h, and marked the mass of the completely dry sample as m_d. The value of total porosity P can be calculated by following:

$$P = \frac{m_s - m_d}{\rho_w V} \quad (2)$$

where $(m_s - m_d)$ is the mass change of sample, g; ρ_w is the density of water; V *is* the volume of the specimen, mm^3.

Microscopic test

After the specimen was broken, specimens of the surface layer were selected, soaked in absolute anhydrous ethanol for 24 h to stop further hydration. Then thermo-gravimetric analysis (TGA), mercury intrusion porosimetry (MIP) and scanning electron microscopy (SEM) were conducted for the microscopic test, respectively. Fresh particles were heated from a setting temperature of 20 °C to 1000 °C with a rate of 10 °C/min by the TGA–DSC I type thermal analyzer. The Auto Pore IV9500 mercury porosimeter was used to measure the pore structure of cover concrete with a maximum pressure of 228 MPa and a contact angle of 130°. The micro-morphology of samples was observed by Nova Nano SEM–50 scanning electron microscope at a scanning frequency of 50/60 Hz.

3 Results and discussion

3.1 Influence of curing methods on water absorption of cover concrete

The changes in water absorption of cover concrete with capillary absorption time, curing method and water binder ratio are shown in **Figure 2** and **Figure 3**. As the absorbing water time increases, the water absorption of cover concrete increases significantly, but the later growth decreases slowly, which is in accordance with the process followed by a bilinear change of capillary water absorption described by Liu's results [31]. The capillary water absorption of all samples with wet-cured methods such as standard curing and water curing is higher than that of dry-cured methods like natural curing and cover curing, which shows that the permeability of cover concrete to a large extent is governed by its curing method. Under natural conditions, in a low humidity environment (below 60% RH), the free water in covered concrete is easy to be evaporated, resulting in water moving into the air and forming water loss channels. The water absorption of standard-cured concrete is minimum, followed by water curing, and the water absorption of cover curing is less than that of natural curing. After de-moulding, unhydrated cement particles will further hydration, through timely and effective wet curing, replenishing rapidly the water consumed by hydration in the matrix, which is beneficial to improve the hydration degree and compactness of cover concrete. This indicated that a suitable curing method is detrimental to the permeability of cover concrete. It is worth noting that the water absorption of samples with water curing keeps higher than that with standard curing. The hydrate is alkaline, and the cement hydration products are dissolved because of the corrosion of water. Especially for $Ca(OH)_2$ with large solubility, it is dissolved first, resulting in the formation of more pores, thereby reducing the impermeability of cover concrete [32,33]. Furthermore, water absorption of samples tends to have results affected by the water binder ratio and the type of cementing material. Comparing **Figure 2** and **Figure 3**, it can be observed that the water absorption of the 0.45 water-binder ratio is greater than that of the 0.35 water-binder ratio. The curing methods affect the water absorption to different degrees for diverse types of cementing material. For S40 samples, water absorption of natural curing is increased by 37%-60% as compared to that of standard curing. For OPC samples, water absorption of natural curing is 15%-40% higher than that of standard curing. The extent to which different cementing materials endure in the erosion process varies, and cementing material system with high-volume slag has a high resistance to water erosion [34]. Owe to high pozzolanic reactivity, slag reacts with $Ca(OH)_2$ in the matrix to generate C-S-H, which results in a significant decrease in the content of $Ca(OH)_2$ in the matrix, avoiding a large amount of $Ca(OH)_2$ dissolution.

It is found that the curve of water absorption for

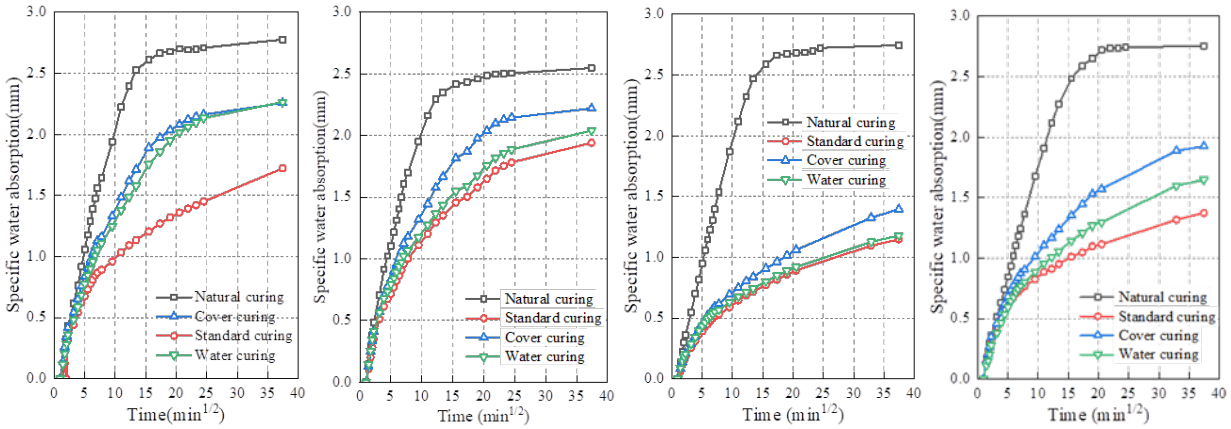

Figure 2. Influence of the curing methods on the 7-day water absorption of specimens when water-binder ratio is 0.35.

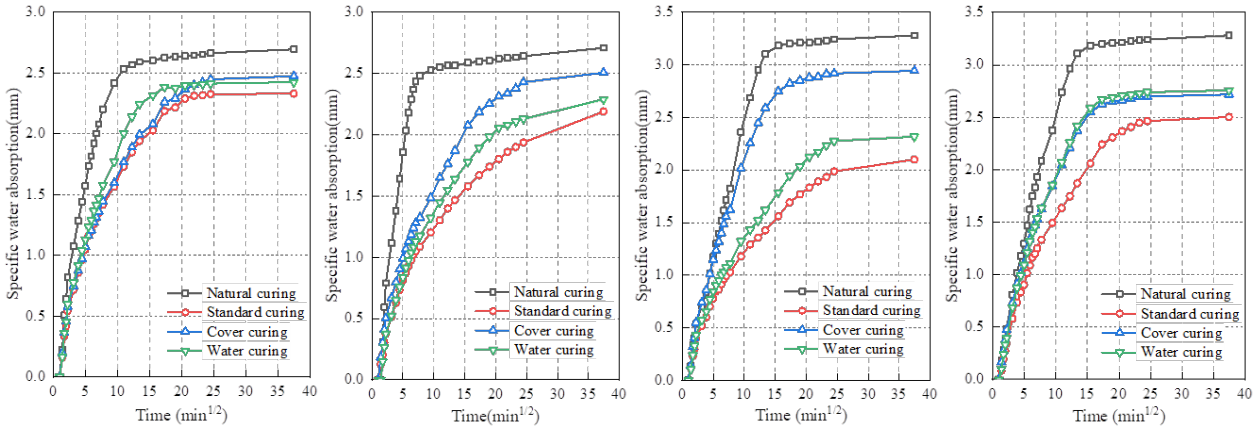

(a) OPC (b) FA30 (c) S40 (d) FA15S20

Figure 3. Influence of the curing methods on the 7-day water absorption of specimens when water-binder ratio is 0.45.

all samples shows a two-stage change. Therefore, the sorptivity coefficient of the samples is calculated using the slopes of the water absorption/square root of time ($t^{0.5}$) curves in the early stage to characterize the strength of permeability [35]. **Figure 4** gives the sorptivity coefficient variation of cover concrete with different curing methods and water-binder ratios. As is shown in the picture, the sorptivity coefficients of cover concrete with a water binder ratio fixed at 0.45 are all greater than that of a water binder ratio fixed at 0.35. This phenomenon can be explained by the high water-binder ratio mixtures having a larger initial water-filled space, namely a large amount of porosity, which provides more paths for water to penetrate into the matrix. The changes in sorptivity coefficients of different curing methods are the same as the water absorption, which manifests as the trend of standard curing < water curing < cover curing < natural curing. Covering concrete with different curing methods has a great influence on the sorptivity coefficient, particularly in FA30, and the average value of the sorptivity coefficient of FA30 with standard curing is 1/2-3/5 of that with natural curing conditions. However, compared with pure cement, the cover concrete of FA30 has a higher sorptivity coefficient under all curing methods. When the water-binder ratio is 0.35, the addition of slag can significantly reduce the sorptivity coefficient of cover concrete, while when the water-binder ratio is 0.45, there is no significant difference in sorptivity coefficient between the OPC and the S40. Since the sorptivity coefficient of cover concrete is greatly impacted by its hydration degree and water-binder ratio, according to the mixture ratio, TGA measure-

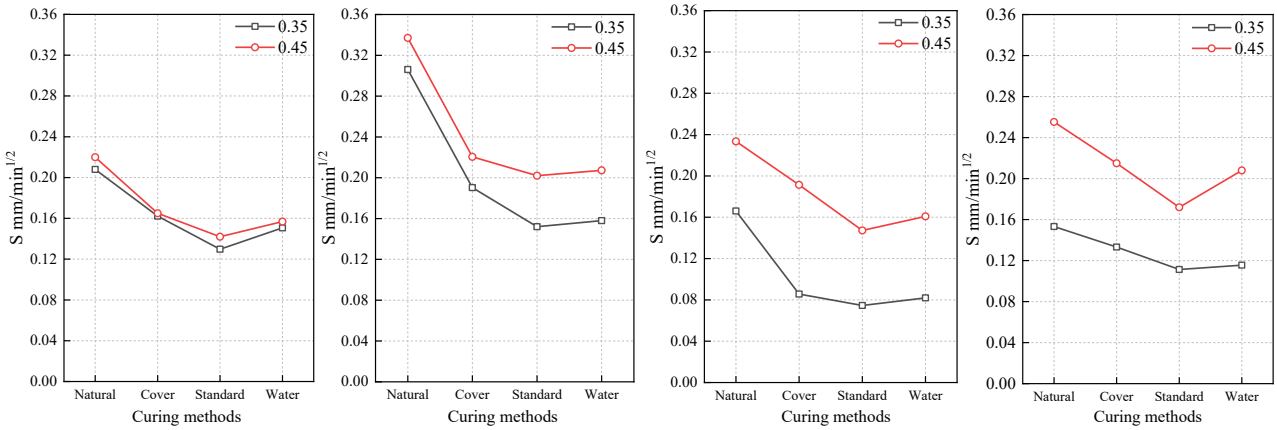

(a) OPC (b) FA30 (c) S40 (d) FA15S20

Figure 4. Influence of the curing methods on the 7-day sorptivity coefficient.

ment was applied to test the hydration properties, and the results are shown in **Figure 5**.

The DTG curves of the samples at 7 days are presented in **Figure 5**, and several typical peaks can be observed in DTG curves. The first endothermic peak existing at about 60-300 °C is attributed to the water loss and disintegration of ettringite and C-S-H gel. One peak occurring between 400-550 °C is caused by the decomposition of $Ca(OH)_2$, and the weight loss of a small amount of calcite appeared at 700 °C [10]. As can be seen in **Figure 5a** cement blended with slag has more hydration products, and results in a higher degree of hydration, so the hydrated body is more compact. That explains why the sorptivity coefficient of cement mixed with slag is half that of pure cement. In contrast, the content of hydration products of cement mixed with fly ash is lower due to the poor reactivity of fly ash [36], which leads to showing a higher water absorption and low impermeability in the capillary water absorption test. However, research has shown that the sorptivity coefficient of cement blended with fly ash continues to decrease with the prolongation of curing time and the development of the pozzolanic reaction [37]. In addition, according to the calculated $Ca(OH)_2$ content data in **Table 4**, it can be observed that with the increase of the water binder ratio, the amount of $Ca(OH)_2$ increases. At a constant water binder ratio, different cementing material systems display various permeability characteristics, and the main difference comes from the different hydration degrees. But it is difficult to explain the change of water absorption between samples with various water-binder ratios, so it needs to be described through the pore structure for further analysis.

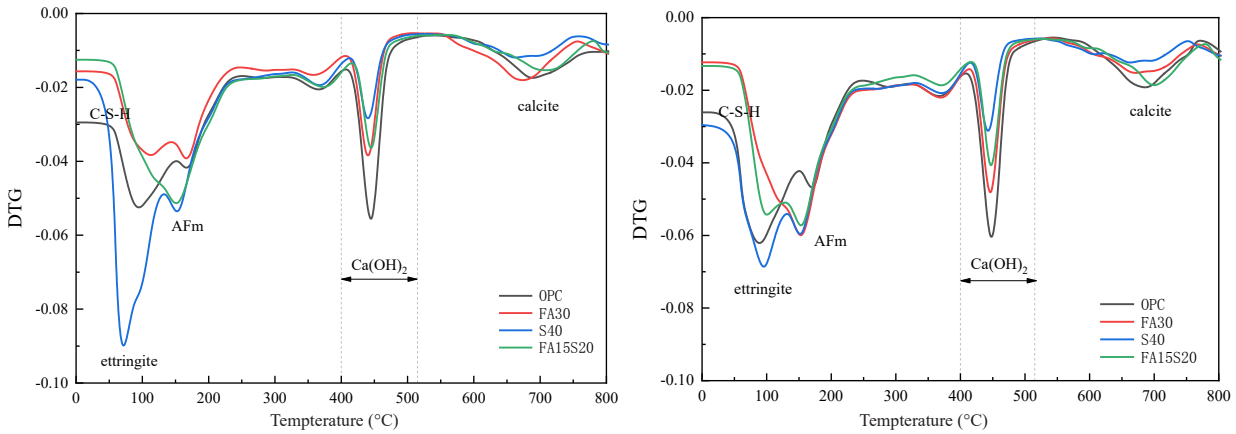

(a) 0.35 (b) 0.45

Figure 5. DTG curves of specimen at 7 days.

Table 4. Calculation value of $Ca(OH)_2$ content for different specimens.

W/C	code	Endothermic peak/°C		Corresponding weight /%		Weight loss(H_2O)/%	CH/%
		Inital	Final	W_1	W_2	W_1–W_2	W_{CH}
0.35	OPC	407.95	504.63	89.97	87.61	2.36	9.70
	FA30	407.78	504.67	91.97	90.34	1.63	6.70
	S40	407.78	504.43	87.56	86.23	1.33	5.47
	FA15S20	417.95	514.55	90.40	88.87	1.53	6.29
0.45	OPC	408.10	543.31	88.73	85.88	2.85	11.76
	FA30	408.26	533.86	90.38	88.24	2.14	9.04
	S40	415.33	523.96	87.73	86.36	1.37	5.63
	FA15S20	416.89	523.92	89.63	87.92	1.72	7.07

3.2 Influence of curing methods on pore structure of cover concrete

Some studies have shown that the permeability of cover concrete is directly related to its pore structure [38,39]. The 7-day total porosity from the exposed surface of the specimens measured by the vacuum saturation test under different curing methods is shown in **Figure 6**. It is easy to find that the porosity of the mixtures with a 0.45 water-binder ratio is significantly greater than that with a 0.35 water-binder ratio. This explains why increasing the water-binder ratio from 0.35 to 0.45 results in the water absorption and sorptivity coefficient of cover concrete increases. Besides, the curing method has a significant effect on the porosity of the specimens. The standard-cured cover concrete is the lowest, followed by the cover curing and water curing, and natural-cured cover concrete has the highest porosity, which indicates that proper curing methods can reduce the total porosity of cover concrete, thereby reducing permeability. However, the experimental results also show that the influential level of the curing method is distinct from the total porosity of different cementing material systems. For cover concrete of pure cement, the total porosity of natural curing is about 17%, which is higher than that of wet curing by 25%; for cement blended with fly ash, the total porosity of natural curing is higher than that of wet curing by 20%-40%; for slag, it is higher about 20%-50%. Thus, the pore structure development of concrete with high-volume mineral admixtures is more sensitive to the curing methods.

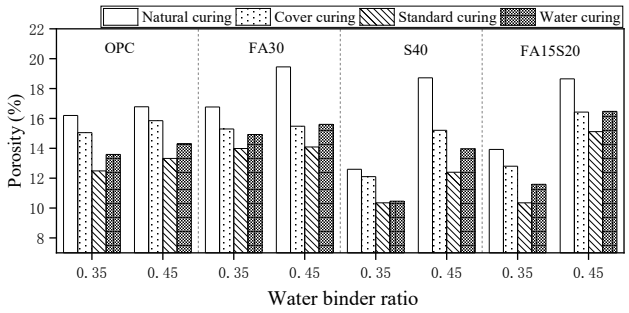

Figure 6. The 7-day total porosity of specimens with different curing methods.

The pore size distribution of cover concrete with different curing methods is characterized by MIP and is presented in **Figure 7**. As shown in **Figure 7**, the pore size is mostly distributed below 50 nm, which is defined as harmless pores and less harmful pores, having little impact on the permeability of the cover concrete. It is proved that the addition of high-volume mineral admixtures tends to increase the maximum pore size of the sample. The pore size of pure cement is mainly distributed in 7-14 nm, and that of cement blended with fly ash and slag is mainly distributed in 11-17 nm and 6-32 nm. Comparing the pore structure of specimens under standard curing and natural curing methods, it can be seen that the proportion of harmless pores and less harmful pores decreases. The pore size distribution curves of natural curing shift right, and as the proportion of macropore of the sample increases, the internal pore tends to be connected. This indicates that the loss of water in the sample of natural curing makes the pore structure of cover concrete much coarser, which is not conducive to the development of compactness. Especially for the cement mixed with slag, the pore structure coarsening of natural curing is the most significant.

3.3 Mechanism discussion on the permeability of cover concrete based on SEM

The curing method has a crucial influence on the microstructure development of cover concrete. For further study on the mechanism of the permeability of cover concrete, the microstructure of cover concrete under natural curing and standard curing was tested by SEM. Typical morphologies of cement main hydration products such as ettringite and $Ca(OH)_2$ cannot be identified from SEM images [40], but it can find out the difference in the effect of curing methods on microscopic morphology. As can be seen from **Figure 8**, the cover concrete is loose and porous under natural curing, and the hydrate has lots of pores and micro-cracks, which are related directly to the process of water loss under the condition of low humidity. Compared with natural curing, the microstructure of standard-cured cover concrete is relatively compact and has no cracks, which explains

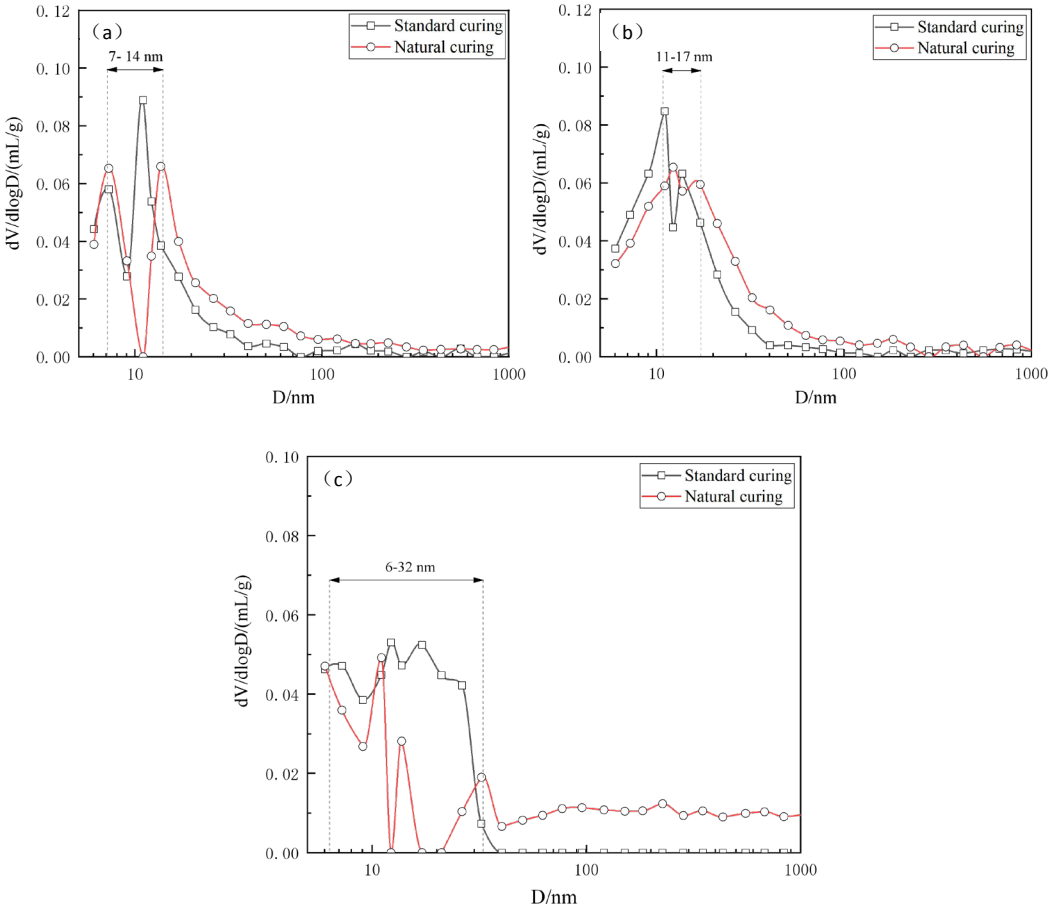

Figure 7. The pore structure of specimens with different curing methods: (a) OPC; (b) FA30; (c) S40.

why standard curing is beneficial to the improvement of impermeability at a micro level. Besides, cementing material type influences microscopic morphology. From the distribution of hydration products, the arrangement of hydration products of cement blended with mineral additive is more uniform and orderly due to the decrease of $Ca(OH)_2$ content. From both images in **Figures 8b and 9b**, the hydrate of cement blended with fly ash has lots of micro-pores. In comparison, the micro morphologies of pure cement pastes and pastes containing slag are more compact, which is in accordance with the result of the higher sorptivity coefficient of the mixture with fly ash.

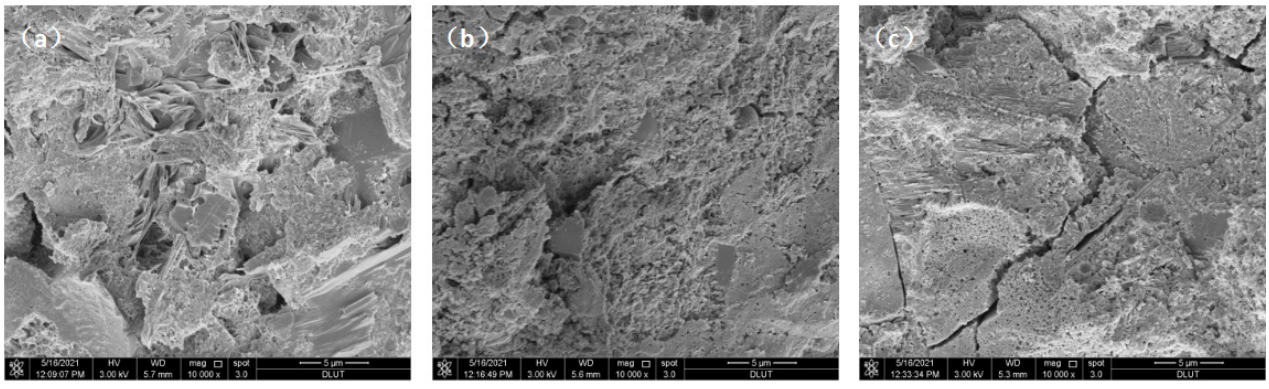

Figure 8. Morphologies of cover concrete with natural curing: (a) OPC; (b) FA30; (c) S40.

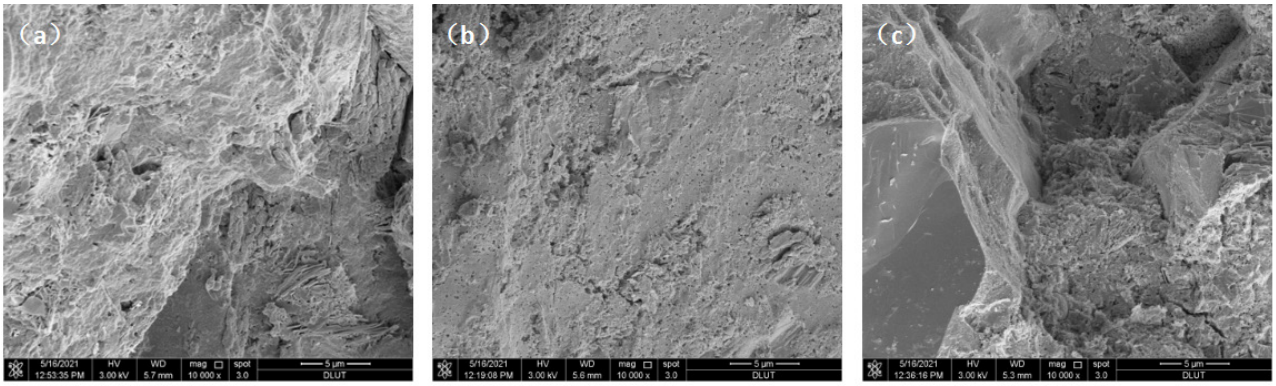

Figure 9. Morphologies of cover concrete with standard curing: (a) OPC; (b) FA30; (c) S40.

4. Conclusions

Based on the results and the discussion of water absorption, sorptivity coefficient, and pore structure of the cover concrete, the following conclusions are drawn:

(1) Strengthening curing has an obvious positive effect on water absorption of cover concrete. For four different curing methods, the water absorption and sorptivity coefficient of cover concrete with natural curing is the maximum, followed by cover curing and water curing, and standard curing is the maximum.

(2) There is a big difference in the water absorption property among the various cementing materials system. Under identical curing conditions, the FA30 performs higher with sorptivity coefficient when compared to the S40. The results obtained by TGA show that the early-age permeability of FA30 is the maximum, which is caused by the low pozzolanic reactivity of fly ash. As the activity of slag is higher than that of fly ash, the anti-permeability of cover concrete of S40 is considerably higher than that of FA30.

(3) There is a clear correlation between the pore structure and water absorption property. The porosity of cover concrete with natural curing is the maximum because of the increase in interconnected pores caused by moisture exchange, and the water absorption is correspondingly the highest. From SEM images, compared to natural curing, the matrix of standard curing is denser.

(4) Proper curing methods can improve the impermeability of cover concrete, and cement with mineral admixtures is more sensitive to curing methods. The reason is that the porosity and pore structure of samples mixed with mineral admixtures are more susceptible to curing methods than pure cement samples.

Conflict of Interest

The author(s) declared no potential conflicts of interest with respect to the research, authorship, and/or publication of this article.

Funding

The authors would like to acknowledge the financial support provided by the National Key R&D Program of China (Grant number2018YFB1600100) and this study is also funded by Shandong Transportation Science and Technology Plan (grant number 2018B44).

References

[1] Austin, S.A., Robins, P.J., Aleesa, A., 1997. Influence of early curing on the sub-surface permeability and strength of silica fume concrete. Magazine of Concrete Research. 49(181), 371-373.

[2] Sajedi, F., Razak, H.A., Mahmud, H.B., et al., 2012. Relationships between compressive strength of cement-slag mortars under air and water curing regimes. Construction & Building Materials. 31, 188-196.

[3] Reinhardt, A., 1997. Gas permeability coefficient of cover concrete as a performance control. Materials and Structures. 30, 387-393.

[4] Ahari, R.S., Erdem, T.K., Ramyar, K., 2015. Permeability properties of self-consolidating concrete containing various supplementary cementitious materials. Construction & Building Materials. 79, 326-336.

[5] Sisomphon, K., Franke, L., 2007. Carbonation rates of concretes containing high volume of pozzolanic materials. Cement & Concrete Research. 37(12), 1647-1653.

[6] Uysal, M., Yilmaz, K., Ipek, M., 2012. The effect of mineral admixtures on mechanical properties, chloride ion permeability and impermeability of self-compacting concrete. Construction & Building Materials. 27, 263-270.

[7] Al-Gahtani, A.S., 2010. Effect of curing methods on the properties of plain and blended cement concretes. Construction & Building Materials. 24(3), 308-314.

[8] Liu, B., Luo, G., Xie, Y., 2018. Effect of curing conditions on the permeability of concrete with high volume mineral admixtures. Construction & Building Materials. 167(10), 359-371.

[9] Nolan, P., 2001. Near-surface moisture gradients and in situ permeation tests. Construction & Building Materials. 15(2-3), 105-114.

[10] Liu, B., Shi, J., Sun, M., et al., 2020. Mechanical and permeability properties of polymer-modified concrete using hydrophobic agent. Journal of Building Engineering. 31, 101337.

[11] Gueneyisi, E., Gesoglu, M., Oezturan, T., et al., 2009. Estimation of chloride permeability of concretes by empirical modeling: considering effects of cement type, curing condition and age. Construction & Building Materials. 23(1), 469-481.

[12] Han, F., Song, S., Liu, J., et al., 2021. Effect of water/binder ratio and temperature on the hydration heat and properties of ternary blended cement containing slag and iron tailing powder. Journal of Thermal Analysis & Calorimetry. 144(4), 1115-1128.

[13] Sabir, B.B., Wild, S., 1998. A water sorptivity test for martar and concrete. Materials and Structures. 31(8), 568-574.

[14] Barnett, S.J., Soutsos, M.N., Millard, S.G., et al., 2006. Strength development of mortars containing ground granulated blast-furnace slag: Effect of curing temperature and determination of apparent activation energies. Cement & Concrete Research. 36(3), 434-440.

[15] Escalante, J.I., Gomez, L.Y., Johal, K.K., et al., 2001. Reactivity of blast-furnace slag in Portland cement blends hydrated under different conditions. Cement & Concrete Research. 31(10), 1403-1409.

[16] Jiang, R., 2020. Influence of early curing method on properties of ultrahigh-performance concrete. Journal of the Chinese Ceramic Society. 48(10), 10.

[17] Shi, H., Xu, B., Zhou, Z., 2009. Influence of mineral admixtures on compressive strength, gas permeability and carbonation of high performance concrete. Construction & Building Materials. 23, 1980-1985.

[18] Shi, M., Wang, Q., Zhou, Z., 2015. Comparison of the properties between high-volume fly ash concrete and high-volume steel slag concrete under temperature matching curing condition. Construction & Building Materials. 98, 649-655.

[19] Shi, J., Liu, B., Wu, X., et al., 2020. Effect of steam curing on surface permeability of concrete: Multiple transmission media. Journal of Building Engineering. 32, 101475.

[20] Wang, Z., Wang, J., Zhu, J., et al., 2020. Energy dissipation and self-centering capacities of posttensioning precast segmental ultra-high performance concrete bridge columns. Structural Concrete. (4), 1-16.

[21] Long, G., He, Z., Omran, A., 2012. Heat damage of steam curing on the surface layer of concrete. Magazine of Concrete Research. 64(11), 995-1004.

[22] Bai, J., Wild, S., Sabir, B.B., 2002. Sorptivity and strength of air-cured and water-cured PC–

PFA–MK concrete and the influence of binder composition on carbonation depth. Cement & Concrete Research. 32(11), 1813-1821.

[23] Tan, K., Gjorv, O.E., 1996. Performance of concrete under different curing conditions. Cement & Concrete Research. 26(3), 355-361.

[24] Gonen, T., Yazicioglu, S., 2007. The influence of mineral admixtures on the short and long-term performance of concrete. Building & Environment. 42(8), 3080-3085.

[25] He, Z., Long, G., Xie, Y., 2012. Influence of subsequent curing on water sorptivity and pore structure of steam-cured concrete. Journal of Central South University. 19(4), 1155-1162.

[26] Lafhaj, Z., Goueygou, M., Djerbi, A., et al., 2006. Correlation between porosity,permeability and ultrasonic parameters of mortar with variable water/cement ratio and water content. Cement & Concrete Research. 36(4), 625-633.

[27] Khatib, J.M., Mangat, P.S., 1995. Research, absorption characteristics of concrete as a function of location relative to casting position. Cement & Concrete Research. 25(5), 999-1010.

[28] Baris, O., Hulusi Ozkul, M., 2004. The influence of initial water curing on the strength development of ordinary Portland and pozzolanic cement concretes. Cement & Concrete Research. 34(1), 13-18.

[29] ASTM C1585. Standard Test Method for Measurement of Rate of Absorption of Water Hydraulic-Cement Concretes [Internet]. Available from: https://www.astm.org/c1585-20.html

[30] Shafiq, N., Cabrera, J.G., 2004. Effects of initial curing condition on the fluid transport properties in opc and fly ash blended cement concrete—sciencedirect. Cement & Concrete Composites. 26(4), 381-387.

[31] Liu, B., Jiang, J., Shen, S., et al., 2020. Effects of curing methods of concrete after steam curing on mechanical strength and permeability. Construction & Building Materials. 256(12), 119441.

[32] Duong, V.B., Sahamitmongkol, R., Tangtermsirikul, S., 2013. Effect of leaching on carbonation resistance and steel corrosion of cement-based materials. Construction & Building Materials. 40, 1066-1075.

[33] Jain, J., Neithalath, N., 2009. Analysis of calcium leaching behavior of plain and modified cement pastes in pure water. Cement & Concrete Composites. 31, 176-185.

[34] Han, F., Liu, R., Yan, P., 2014. Effect of fresh water leaching on the microstructure of hardened composite binder pastes. Construction & Building Materials. 68(15), 630-636.

[35] Benli, A., Karatas, M., Bakir, Y., 2017. An experimental study of different curing regimes on the mechanical properties and sorptivity of self-compacting mortars with fly ash and silica fume. Construction & Building Materials. 144(30), 552-562.

[36] Wang, Q., Li, M., Jiang, G., 2014. The difference among the effects of high-temperature curing on the early hydration properties of different cementitious systems. Journal of Thermal Analysis & Calorimetry. 118(1), 51-58.

[37] Tasdemir, C., 2003. Combined effects of mineral admixtures and curing conditions on the sorptivity coefficient of concrete. Cement & Concrete Research. 33(10), 1637-1642.

[38] Gonzalez-Corominas, A., Etxeberria, M., Poon, C.S., 2016. Influence of steam curing on the pore structures and mechanical properties of fly-ash high performance concrete prepared with recycled aggregates. Cement & Concrete Composites. 71, 77-84.

[39] Nguyen, M.H., Nakarai, K., Nishio, S., 2019. Durability index for quality classification of cover concrete based on water intentional spraying tests. Cement & Concrete Composites. 104, 103355.

[40] Rong, Z.D., Sun, W., Xiao, H.J., et al., 2014. Effect of silica fume and fly ash on hydration and microstructure evolution of cement based composites at low water-binder ratios. Construction & Building Materials. 51, 446-450.

BILINGUAL PUBLISHING GROUP

Journal of Building Material Science

https://journals.bilpubgroup.com/index.php/jbms

ARTICLE

Cost Comparison of Different Types of Formworks

Kiran Devi* *, *Tushar Yadav

Department of Civil Engineering, SGT University, Gurugram, Haryana, 122505, India

ABSTRACT

Formwork is the temporary moulds in the construction which is fabricated based on the drawing and design of the structure and into which the concrete is poured to form the required structure. Formwork is an essential part of the construction as it has been used by the Romans. The formworks must be strong enough to withstand all types of loads. The joint must be in proper condition to avoid any kind of leakages. The materials used for the formworks should be economical, easily available and durable. The formworks can be made up of different materials such as plywood, steel, aluminum, composite material, etc. In steel formwork the plates used for the slab support are made up of galvanized steel and these are fabricated as per the requirements. Aluminum plates are used in the aluminum framework along with the other components made up of aluminum. The selection of a suitable framework is important in any project because it bears about 25% to 30% cost of the total cost of construction. In the present study, different types of formworks such as steel, plywood and aluminum were studied in a project and a comparison was made on the reusability and easiness in handling and maintenance. Also, a comparison of the formwork used in the construction of the 5th and 11th-floor tower based on the specific plan and drawing was done. The results showed that the aluminum formwork was found to be efficient and suitable among all formworks, although the cost was higher compared to other formwork materials.

Keywords: Formworks; Steel formworks; Plywood formworks; Aluminum formworks; Cost analysis

1. Introduction

Formwork is a mould-like container into which fresh concrete is poured and compacted. When the concrete is set, the formwork is removed and a solid mass is obtained in the shape of the inner face of the formwork. Generally, the top of the formwork is left

*CORRESPONDING AUTHOR:

Corresponding Author: Kiran Devi, Department of Civil Engineering, SGT University, Gurugram, Haryana, 122505, India; Email: kiran-bimbhra@gmail.com

ARTICLE INFO

Received: 6 March 2023 | Revised: 30 March 2023 | Accepted: 10 April 2023 | Published Online: 15 April 2023

DOI: https://doi.org/10.30564/jbms.v5i1.5515

CITATION

Devi, K., Yadav, T., 2023. Cost Comparison of Different Types of Formworks. Journal of Building Material Science. 5(1): 32-38. DOI: https://doi.org/10.30564/jbms.v5i1.5515

open. The geometry realisation and strength development of concrete elements are greatly assisted by formwork. The formwork used to cast the structural elements such as, columns, beams and slabs, is also used for smaller parts of the building such as stairs. Formwork in the building is a crucial task that calls for exceptional accuracy and ability. Lack of precision and ability during formwork building may result in a poor and unsatisfactory quality of work, which ultimately causes a loss of important resources like time and money. The formwork is carefully removed when the concrete has matured and becomes hard. The process of removal of formworks is known as stripping. A good formwork should be able to withstand the forces being applied to it either during or after the concreting process. There is no slurry leakage in the formworks. The surface of a good formwork should be smooth and wrinkle-free after the stripping, consequently producing superior quality and a smoother final concrete product. It should be sturdy enough to be used repeatedly. The causes of failure of formworks are overloading of any props, failure of shuttering due to excessive vibrations of needle surface vibrators, failure due to improper supervision, inadequate design/planning of shuttering, centring and concreting activity [1-3].

The materials used for the formworks are steel, timber, plywood, aluminium, composite materials, etc. Plywood is the manufactured product of timber and consists of veneer sheets or piles in layers. Plywood as formwork material is used due to its smooth finish, lightweight, strong and low finishing cost. The plywood formwork consists of a plyboard, batten, wooden props (balls), nails, binding wires, shuttering oil, clamps, wooden batten (channel), scaffolding. Steel formworks are used in mass structures such as dams, and bridges and provide an excellent finish to the concrete surface and can be reused numerous times. It is strong, easy to dismantle but the cost is higher, corrosion may occur and need the use of lifting equipment due to its heavy weight. Steel is also used for the purpose of formwork. It is quite costly but can be used more times. They are used in structures like dams, bridges, etc. Steel shuttering is installed using clamps, bolts and nuts. They are comparatively heavy compared to other types of formwork. Panels comprised of thin steel plates that are attached around the edges by tiny steel angles make up steel formwork. Aluminium formworks are used in the prefabricated structure. It is lightweight, needs lesser support, is reusable and has good strength. Similarly, aluminium is the major material in the aluminium formwork. It is also known as the Mivan Formwork. The material used is a certain type of aluminium alloy that has the resistive property against different atmospheric conditions like wet, dry, humid. aluminium as a metal is corrosion free as it reacts with the oxygen present in the atmosphere and forms an aluminium oxide layer which prevents corrosion. Although the initial cost for the fabrication is high it has a high reusability factor, which is it can be reused more times compared to the plywood formwork, which compensates for the high investment cost. The components of aluminium formwork are aluminium panel, pin and wedge, tie rod, wing nuts, kicker, wall tie, vertical soldier, slab mounted brackets, external corner, props, wall attach bracket, scaffolding. When using the flat tie and casting concrete together, a stub pin and wedge are needed. Wall ties, pins, and wedge bolts are used with construction formwork accessory wedge to secure the formwork. In the present study, different materials of formworks such as steel, plywood and aluminium were studied and a comparison was made in terms of cost.

Patil and Mundhada [4] compared the Mivan or aluminum formwork with the conventional formwork. Results showed that the finish obtained from the Mivan formwork was very good and did not require any plasterwork compared to conventional formwork.

Aluminium and steel formwork are fairly comparable to one other. Of course, aluminium makes up the majority of it. The primary distinction between steel and aluminium formwork is that the aluminium is having lesser weight as compared to steel. This is due to the fact that aluminium has a lower density than steel which makes it easier to handle [5].

Terzioglu et al. [6] conducted an analysis that deals

with the criteria which need to be used in order to select the formwork but it does not provide anything related to cost in terms of choosing the formwork and also regarding the quantity of the components. Shrivastava et al. [7] conducted an analysis of planning of formwork materials by which analyses the formwork materials which are used will depend upon the type of building, whether the building is commercial, residential, factory or industrial or another type of building. The selection of the kind of formwork is in it itself a big task and it affects the overall cost of the project. It is one of the major inputs which also affects the design of the building as well. This paper will discuss what kind of formwork materials should be selected for different building typologies. Li et al. [1] conducted a review of formwork systems for modern concrete construction which presents a comprehensive review of various formwork systems in concrete construction, including their raw materials, flexibility, fabrication methods, applications in concrete structures and environmental impacts.

The objectives of the present study are to analyse a) components used in the different kinds of formwork: Plywood, steel and aluminium, b) the quantity of the components used in the formwork and c) the components that are used in the formwork. After doing all these at last a comparison has been made among the three formworks in order to choose the best as compared to others. Very few studies are available on the cost comparison of different formworks i.e. steel, plywood, aluminum formworks and their components used for a 2 BHK project. The number of formworks required during the project and their cost were calculated and compared manually.

2. Methodology

In the present study, the design of the floor of the area was calculated manually. The floor plan includes 2 BHK along with the drawing room has been shown in **Figure 1**. After calculating the total area for which the formwork is required manually, the slab area of each floor was calculated. After knowing the area from the plan manually, the total number of plywood, steel and aluminium plates required to

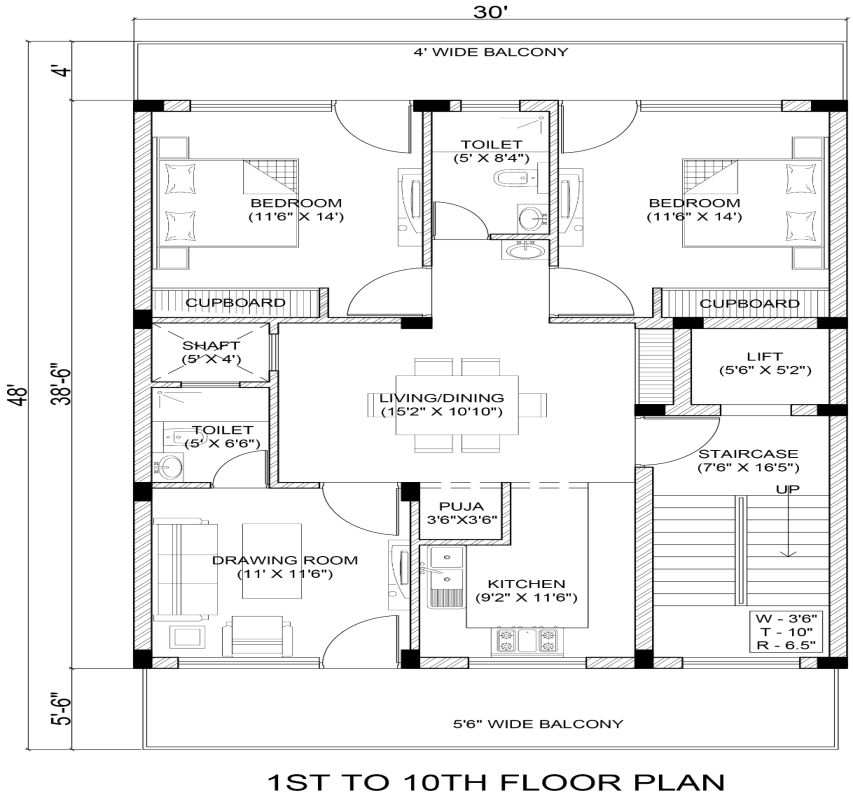

Figure 1. Floor plan.

cover the slab area is calculated manually. Also, the total number of columns and beams to be constructed per floor is calculated. Then based on the calculation the total number of props, channels and other components used to support the concrete for the construction of these elements on the building. All the calculation was done manually. After knowing the quantity of the components that is required. The respective prices and the cost of each component are researched as per the local market. In addition to the formwork it also involves the cost and analysis of the components of the scaffolding required for the construction. For the plywood and steel formwork the rate list is collected based on the components that are used in the analysis. For the Mivan formwork the rates of the component were gathered from the vendor Winntus Formwork Private Limited. For the components used in the scaffolding the rates are collected from the local vendor and then calculated the total cost of the scaffolding is based on the components used. The flow chart of the methodology has been shown in **Figure 2**.

3. Results

The different materials i.e., steel, plywood and aluminum formworks were used in a project and a cost comparison was carried out. Calculation of aluminium formwork was done on a square metre basis. The rate of aluminium panels was Rs 7000 per square metre. Note: The moulds of aluminium formwork were manufactured as per drawings. The different members were used in plywood, steel and aluminum formwork and their prices have been given in **Tables 1a, 1b, 2 and 3** respectively. The total cost of different formworks was evaluated for a particular project and a comparison was made.

It has been observed from **Figure 3** that the cost of the scaffolding of all three formworks is similar whereas the total cost of plywood formwork was least followed by steel and aluminium formwork. However, the overall cost of aluminium formwork was minimum and steel formwork was the maximum among all the formworks.

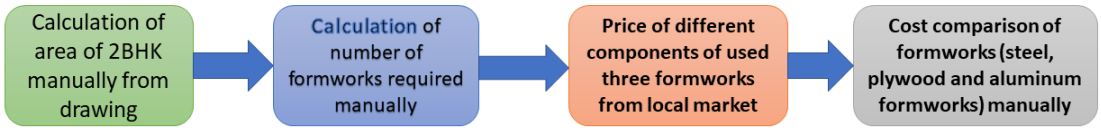

Figure 2. Flow chart for the cost comparison of formworks.

Table 1a. Cost of different members of plywood formworks.

Plywood formwork				
Sr. No.	Member	Total no. of member	Price (Rs.)	Total cost (Rs.)
1	Plywood (Beam, Column, Slab)	93	1550	144150
2	Batten (Beam, Column)	371	195	72345
3	Batten (Slab)	192	185	35520
4	Wooden batten	39	550	21450
5	Prop (Beam)	96	135	12960
6	Prop (Slab)	156	145	22620
7	Clamps (Beam, column)	336	150	50400
8	Ledger	296	680	212080
9	Base Jack	16	190	3040
10	Challi	24	1540	36960
11	Base jack	22	190	4180
12	Challi	36	1540	55440

Table 1a continued

	Scaffolding	Length	Cost of scaffolding	Total cost
1	Length of standard	208*3 = 624	680	424320
2	Length of ledger	518*1.5 = 777	680	528360
3	Guard rail	24	680	16320
4	Length of bracing	39	680	26520
5	Length of standard	286*3 = 858	680	583440
6	Ledger	740*1.5 = 1110	680	754800
7	Ledger	296*1 = 296	680	201280
8	Guard rail	34	680	23120
9	Length of bracing	45	680	30600
3	Shuttering Oil	19	60	1140

Table 1b. The unit price of different materials.

Sr. No.	**Product**	**Weight (kg)**	**Price (Rs.)**	**Total cost (Rs.)**
1	Nail	28	85	2380
2	Binding wire	4	85	340
3	Shuttering Oil	19	60	1140

Table 2. The number and cost of members in steel formwork.

Steel formwork				
Sr. No.	Member	Number	Cost of member	Total cost
1	Total nos of steel plates (beam, column, slab)	484	1540	745360
2	Total no. of nuts and bolts	685	12	8220
3	Shuttering oil	190 Lit	60	1140
4	No. of Channels	63	1750	110250
5	Total no. of props	348	1400	487200
6	Total no. of scaffolding (30 ft side)	624	680	424320
7	No. of ledger (1.5 m)	777	680	528360
8	No. of ledger (1 m)	296	680	212080
9	No. of base jack	16	190	3040
10	No. of challi	24	1540	36960
11	Guard rail (24 m)	-	680	16320
12	Bracing (39 m)	-	680	26520
13	Total length of standard (scaffolding, 48 ft side)	286	680	583440
14	No. of ledger (1.5m)	740*1.5= 1110	680	754800
15	No. of ledger (1 m)	296	680	201280
16	No. of base jack	22	190	4180
17	No. of challi	36	1540	55440
18	Guard rail (length = 34 m)	-	680	23120
19	Bracing (length = 45 m)	-	680	30600

Table 3. Cost of different aluminum formwork members.

Aluminium formwork				
Sr. No.	Member	Area/no.	Cost per unit	Total cost
1	Area of beam, column, slab	269.64 sq. m.	700	1887480
2	No. of props	186	1400	260400
3	No. of pins and wedge	1210	12.85	15548
4	No. of bracket	32	1700	54400
5	Vol. of shuttering oil	19 lit	60	1140
6	No. of external corner	60	350	21000
7	No. of vertical solider	30	400	12000
8	No. of tie rod	54	90	4860
9	No. of wing nut	60	45	2700
10	Total length of standard (Scaffolding 30ft side)	624	680	424320
11	Length of ledger (1.5 m)	777	680	528360
12	Length of ledger (1 m)	296	680	212080
13	No. of base jack	16	190	3040
14	No. of challi	24	1540	36960
15	Length of guard rail	24 m	680	16320
16	Length of bracing	39 m	680	26520
17	Length of standard (Scaffolding 48 ft side)	858	680	583440
18	Length of ledger (1.5 m)	1110	680	754800
19	Length of ledger (1 m)	296	680	201280
20	No. of base jack	22	190	4180
21	No. of challi	36	1540	55440
22	Length of guard rail	34 m	680	23120
23	Length of bracing	45 m	680	30600

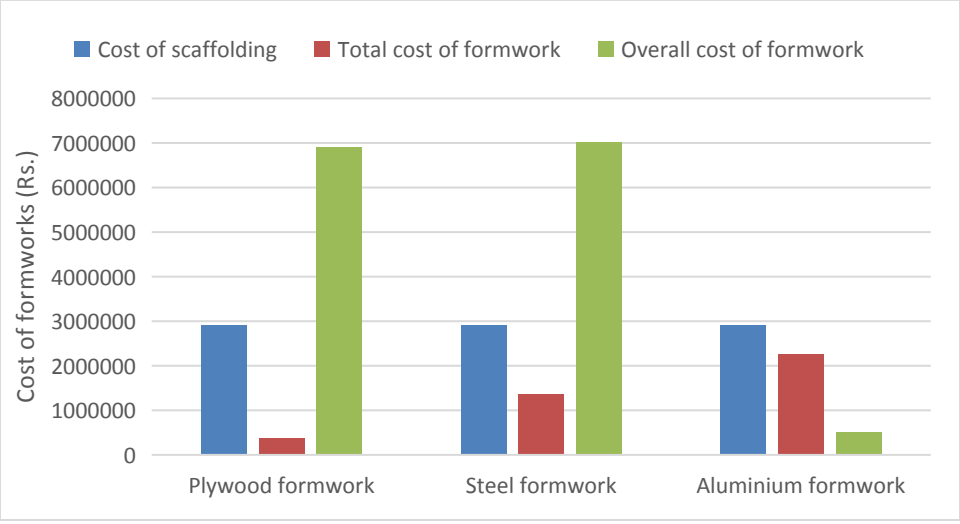

Figure 3. Cost comparison of different formworks.

4. Conclusions

In the present study, different formworks such as plywood, steel and aluminium were used for a project. The calculation of area, number of formworks, cost of formworks and their components were compared manually. The following conclusions were found from the above study:

- The cost of plywood formwork is high because its reusability is very less a number of times, resulting in a higher cost of plywood formwork. Therefore, it is not considered and useful for high-rise or large construction projects.
- The overall cost of steel formwork is highest as compared to plywood and aluminium formwork. In addition to the higher cost, the finishing after deshuttering of the steel formwork is not good and it requires further plastering which contributes to a hike in cost. Also, these formworks are not corrosion-proof, which reduces their strength over a period of time. Due to its heavy weight, it is tough to transfer the steel formwork from one floor to another.
- Aluminium formwork is corrosion resistive, lightweight, easy to handle and transfer and the finishing after deshuttering the formwork is smooth. So, no need for further plastering is required. The initial high cost of aluminium formwork is compensated due to its very high reusability as it can be reused more than 150 times. Due to this the overall cost of the aluminium formwork is less as compared to steel and plywood.
- After considering all the aspects it can be concluded that the aluminium formwork is the most suitable and economical formwork for the construction of high-rise buildings due to its lower cost and good characteristics compared to other formworks.

Author Contributions

Kiran Devi: design and draft of article; and Tushar: concept and analysis of data for the article.

Conflict of Interest

The authors declare that they have no known competing financial interests or personal relationships that could have appeared to influence the work reported in this paper.

References

[1] Li, W., Lin, X., Bao, D.W., et al., 2022. A review of formwork systems for modern concrete construction. Structures. 38, 52-63.

[2] Yudina, A.F., Zhivotov, D.A., Tilinin, Y.I., 2023. Additive technologies for manufacture of formwork. Proceedings of ECSF 2021: Engineering, construction, and infrastructure solutions for unnovative medicine facilities. Springer: Cham. pp. 311-318.
DOI: https://doi.org/10.1007/978-3-030-99877-6_37

[3] Donker, D.K., Mahamud, S., 2022. Comparative assessment of formwork systems used in construction projects in the tamale metropolis of Northern Ghana. SSRG International Journal of Civil Engineering. 9(2), 44-50.
DOI: https://doi.org/10.14445/23488352/IJCE-V9I2P104

[4] Patil, P., Mundhada, P., 2022. Comparative analysis of Mivan formwork and conventional formwork. Smart Technologies for Energy, Environment and Sustainable Development. 2, 239-245.
DOI: https://doi.org/10.1007/978-981-16-6879-1_24

[5] Terzioglu, T., Turkoglu, H., Polat, G., 2021. Formwork systems selection criteria for building construction projects: A critical review of the literature. Canadian Journal of Civil Engineering. 49(4), 617-626.
DOI: https://doi.org/10.1139/cjce-2021-0190

[6] Terzioglu, T., Polat, G., Turkoglu, H., 2021. Analysis of formwork system selection criteria for building construction projects: A comparative study. Buildings. 11(12), 618.
DOI: https://doi.org/10.3390/buildings11120618

[7] Shrivastava, A., Saxena, S., Chourasria, D., 2021. Planning of formwork materials. Materials Today: Proceedings. 47(1), 7060-7063.
DOI: https://doi.org/10.1016/j.matpr.2021.06.121

BILINGUAL PUBLISHING GROUP

Journal of Building Material Science

https://journals.bilpubgroup.com/index.php/jbms

ARTICLE

Evaluation of the Relationship between Bacteria Concentration and the Strength and Durability of Self-compacting Concrete Incorporating *Sporosarcina pasteurii*

***Engr K Taku*[1*], *Amartey, B. H. S.*[2], *Agber, T.*[3]**

[1] *Department of Civil Engineering, Joseph Sarwuan Tarka University, P.M.B 2373, Makurdi, Nigeria*

[2] *Department of Civil Engineering, Ahmadu Bello University, Zaria, 810107, Nigeria*

[3] *Directorate of Physical Planning, Benue State University, Makurdi, 102119, Nigeria*

ABSTRACT

This research was carried out to evaluate the relationship between the incorporation of calcite precipitation bacteria, *sporosarcina pasteurii* using calcium lactate as nutrient source and the properties of calcined clay and limestone powder blended self-compacting concrete. Ten mixes were designed and designated S0 to S9 with S0 the control (without bacteria and nutrient) and S1 to S9 at varying bacteria and calcium lactate concentrations and the effect of the bacteria cell density and calcium lactate concentration on the compressive strength, sorptivity and tensile strength with age were evaluated using experimental program and statistical packages (ANOVA and post hoc tests). The result of both the experimental program and statistical evaluation shows that the incorporation of *sporosarcina pasteurii* and calcium lactate as nutrients had a positive impact on the properties of the ternary blended self-compacting concrete.

Keywords: S*porosarcina pasteurii;* Calcium lactate; Ternary self-compacting concrete; Statistical evaluation; Strength and durability

1. Introduction

Self-compacting concrete is generally the more expensive and less environmentally friendly version of concrete in terms of the high cement content requirement [1]. Since the production of self-compact-

*CORRESPONDING AUTHOR:

Engr K Taku, Department of Civil Engineering, Joseph Sarwuan Tarka University, P.M.B 2373, Makurdi, Nigeria; Email: kumataku@yahoo.com

ARTICLE INFO

Received: 27 March 2023 | Revised: 18 April 2023 | Accepted: 27 April 2023 | Published Online: 4 May 2023

DOI: https://doi.org/10.30564/jbms.v5i1.5596

CITATION

Taku, J.K., Amartey, B.H.S., Agber, T., 2023. Evaluation of the Relationship between Bacteria Concentration and the Strength and Durability of Self-compacting Concrete Incorporating *Sporosarcina pasteurii*. Journal of Building Material Science. 5(1): 39-48. DOI: https://doi.org/10.30564/jbms.v5i1.5596

ing concrete requires the use of large quantities of cement and fines, the former being expensive and eco-unfriendly, this leads to an escalation of the overall cost of construction using this very important construction material. Thus, the production of SCC using the required quantities of cement is not sustainable due to the fact that sustainability can only ensue with the use of cheaply and readily available local construction materials [2]. There is thus a compelling need to use readily available and relatively cheaper cementitious alternatives and fines (fillers) in the production of SCC while not compromising its flowability, filling ability, segregation resistance, and strength as well as durability characteristics of SCC. The use of calcined clay and Limestone powder will alleviate, to a large extent, the cost and environmental effect associated with SCC production, and they have been used successfully in normal vibrated concrete [3]. More so, the durability of SCC can be enhanced by an improvement of its pore structure by positively altering its permeation properties. One way this can be done is by the application of Microbial Induced Calcite Precipitation technology (MICP) in SCC, which could lead to an improvement in the pore characterization of SCC and hence its durability. The combined use of MICP technology via the application of calcite precipitation bacteria and the use of ternary blends of cement, limestone powder and calcined clay will solve multiple problems associated with SCC production and use, namely; environmental impact, economy, strength and durability characterization.

The use of statistics in solving engineering problems is well documented [4]. Statistical packages like ANOVA and post hoc packages like Tukey HSD, Scheffé, Holm and Bonferroni multiple comparison analysis tools can be used to evaluate the extent of the relationships between variables and this act to complement the results of experimental programs.

This research uses ANOVA from Microsoft Excel and post hoc packages from National Institute of Standards and Technology (NIST), US department of Commerce to evaluate the statistical relationship between the incorporation of bacteria in concrete and its effect on the properties of SCC.

2. Methodology

2.1 Preparation of cementation reagent

The following composition was used in the first instance in preparing the cementation reagent.
Nutrient broth (calcium lactate)
Urea: 20 gm
Ammonium chloride: 10 gm
Sodium hydrogen carbonate: 2.12 gm
Calcium chloride: 2.8 gm
Distilled water: 1000 mL

Calcium lactate was used as the nutrient source and it was dissolved in one litre of distilled or sterile water to produce a solution of desired concentration of 0.01 mol/L. Three different quantities of this solution were used corresponding to 0.5, 1.0 and 2.0% by weight of cement. The composition listed above was weighed and dissolved in 1 litre of distilled water in a conical flask and cotton flogged. The media were then sterile in an autoclave at a temperature of 110 °C for 10 minutes allowed to cool before use.

2.2 Bacteria isolation and inoculation

The prepared media are cotton flogged and sterilized in an autoclave at a temperature of 110 °C for 10 minutes, allow the media to cool completely before inoculation of the bacteria. The ureolytic bacteria (*sporosarcina pasteurii)* was isolated from fresh soil by sub-culturing in 1 L of sterilized nutrient bough and the media was incubated at 35 °C in an orbital shaker for 10 days at 125 rpm. The bacteria growth was determined in terms of optical density by measuring the rate of absorbance at a wavelength of 500 nm. The isolate was purified using the streak plate technique on nutrient agar and the bacteria isolate was identified. The quantification of the bacteria was carried out by using a spectrophotometer. A blank solution of 0.5 mL was placed in the spectrophotometer at a wavelength of 500 nm and the reading was taken. The blank solution was replaced by the bacteria solution of 0.5 mL at the same wave-

length and the concentration of the bacteria was measured using the relation $y = 8.59\times10^{7}z^{1.3627}$ where y is the bacterial concentration per mL and z is the reading at OD600. After the media have cooled, the conical flasks are labeled using masking tape then a standardized incubator of the bacterial isolate will be inoculated. A standardized incubator is a bacterial suspension whose turbidity is compared with that of the McFarland turbidity standard. The standard starts from a scale of 0.5 to 9, and each scale is representing a bacteria cell density. After inoculating the media with the standardized bacteria, the conical flasks were incubated in an incubator at a temperature of 37 °C for 24 hours before use. For this research, the bacterial cell density used corresponded to a McFarland turbidity scale of 0.5, 2.0 and 4.0.

2.3 Mix design

The method of mix design that is adapted for this work is based on the plastic viscosity of the SCC mix, which was first proposed by Karihaloo & Ghanbari and Deeb & Karihaloo [5,6]. It exploits the expression for the determination of the plastic viscosity of a heterogeneous material like SCC from the known plastic viscosity of the homogeneous component (in this case the cement paste). It is based on the micromechanical procedure developed by Ghanbari & Karihaloo [7].

For the self-compacting concrete incorporating *sporosarcina pasteurii* and calcium lactate, ten mixes were designed and designated S0 to S9 with S0 the control (without bacteria and nutrients) and S1 to S9 at varying bacteria and calcium lactate concentrations.

Table 1 shows the mix compositions used for developing the different mixes at different bacterial concentrations and nutrient content.

2.4 Strength characterization

The compressive strength of the self-compacting concrete incorporating *Sporosarcina pasteurii* was determined using 100 cubic millimeters of concrete cubes cured at 7, 14, 28 and 56 days in accordance with the provisions of BS EN 12390-3 [8]. For each mix, three cubes were used and the average value was taken, with a total of 120 cubes used in the determination of the compressive strength of the calcined clay and limestone powder blended SCC. Cement was replaced partially with 15% calcined clay and using limestone powder as filler.

The tensile strength was determined using a diameter of 100 by 200 cylinders at 7 and 28 days by means of the split tensile strength test by crushing the cylinders longitudinally on a compressive strength test machine in line with the provisions of BS EN 12390-6 [9]. Three specimens were used for each test and the average value was taken. A total of 60 cylinders were used in the investigation of the tensile strength of the self-compacting concrete incorporating *Sporosarcina pasteurii.*

Table 1. Mix designation and proportions for bio self-compacting concrete.

Mix	Bacteria Conc. Cfu/mL	Calcium lactate (% of cement)	Cement (kg)	Calcined clay (kg)	Superplasticizer (kg)	Limestone filler (kg)	Sand kg	Coarse aggregates
S0	-	-	11.56	2.04	0.083	4.1	25.9	28.3
S1	1.5×10^{8}	0.5	11.56	2.04	0.083	4.1	25.9	28.3
S2	1.5×10^{8}	1.0	11.56	2.04	0.083	4.1	25.9	28.3
S3	1.5×10^{8}	2.0	11.56	2.04	0.083	4.1	25.9	28.3
S4	1.2×10^{9}	0.5	11.56	2.04	0.083	4.1	25.9	28.3
S5	1.2×10^{9}	1.0	11.56	2.04	0.083	4.1	25.9	28.3
S6	1.2×10^{9}	2.0	11.56	2.04	0.083	4.1	25.9	28.3
S7	2.4×10^{9}	0.5	11.56	2.04	0.083	4.1	25.9	28.3
S8	2.4×10^{9}	1.0	11.56	2.04	0.083	4.1	25.9	28.3
S9	2.4×10^{9}	2.0	11.56	2.04	0.083	4.1	25.9	28.3

2.5 Permeation characterization

The permeation properties of the SCC were evaluated using sorptivity which was carried out to determine the susceptibility of the unsaturated concrete to the penetration of water through capillarity by determining the increase in the mass of the specimen resulting from absorption of water as a function of time when only one surface is exposed to water [10]. The test was carried out at 28 and 56 days for each mix to evaluate the short and long-term effects of the SCM and filler materials on the rate of water absorption through interconnected capillary poles. Three diameters 100 by 50 discs, cut from 100 by 200 concrete cylinder specimens, were used for each test and the average result was calculated. A total of 90 discs cut from 30 cylinders were used for the determination of sorptivity for Bio-SCC.

2.6 Statistical validation

The analysis of variance was carried out using statistiXL package in Microsoft Excel while the post hoc tests were carried out using engineering statistical packages from the National Institute of Standards and Technology (NIST), US Department of Commerce.

3. Results and discussion

3.1 Compressive strength relationship

The strength properties of the calcined clay and limestone powder blended self-compacting concrete incorporating *sporosarcina pasteurii* as calcite precipitation agent at different bacterial cell density and nutrient content was measured using compressive strength at 7, 28 and 56 days and tensile strength at 7 and 28 days. The result for the change in compressive strength with age of concrete, bacterial cell density and nutrient content is presented in **Figure 1**. It can be seen from **Figure 1** that the compressive strength changes with the bacterial density, nutrient concentration and age of concrete. Generally, the strength increases as the concrete ages, with the highest strength recorded at 56 days of curing. Also the SCC mix with bacteria and nutrients shows higher strength than the control (without bacteria). This is because, the bacteria, in the presence of moisture, use up the nutrient and deposits calcium calcite which also improves the strength development. This, in addition to cement hydration and the pozzolanic reaction accounts for the improved strength development with age. For a given bacteria concentration, using 0.5% calcium lactate maximized the compressive strength, with a decrease in the rate of strength

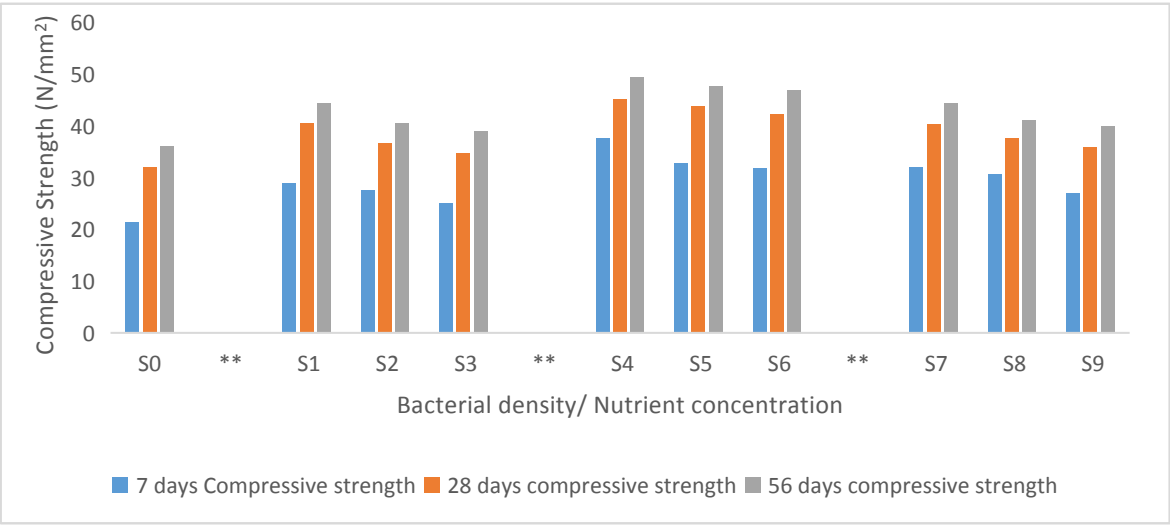

Figure 1. Relationship between bacterial concentration and compressive strength.

development with increasing calcium lactate content. The over-production of calcium carbonate crystals, which lowers the quality of the micro-structure resulted in a lower rate of strength gain at higher calcium content [11].

Also, materials added into concrete that do not contribute to the hydration process could impede strength development [10]. The gain in strength is due to the densification of the pore system due to the precipitation of calcium carbonate by the bacteria cells [11]. According to a recent study, it can be inferred that adding different bacterial concentrations leads to two different types of healing in concrete, namely, surface healing and inner matrix healing. At the surface region, as the availability of water is equal for all the samples, the precipitation is only dependent upon the bacterial concentration. Since a greater number of bacterial cells can precipitate a higher amount of calcite, the maximum amount of precipitation at the surface region of the mortar takes place at the highest cell concentration [12]. Thus, all the test results directly related to the surface region of the mortar, such as surface crack and pore healing and reduction in water penetration depth, exhibit better performance at the highest cell concentration (2.4×10^9 cfu/mL). However, the high calcite precipitation almost blocks the surface pores, and that leads to lower availability of water inside the mortar matrix. This is correlated with the result of research by Mondel & Ghosh, who state that there is an optimal bacteria cell concentration beyond which the strength could be adversely affected [13].

Also, the gain in strength from age 7 to 28 days is higher than that from age 28 to 56 days. This could be due to reduced hydration with age and reduced bacteria activity. Generally, bacteria activity reduces or even stops as the concrete environment gets more alkaline. Thus, with increased hydration and calcium hydroxide production, the concrete matrix gets more alkaline, thereby affecting the bacteria activity and hence calcium calcite production.

Analysis of Variance (ANOVA) was used to evaluate the relationship between the compressive strength, calcium lactate content and bacterial cell density as well as the age of concrete. The null hypothesis postulates that there is no significant relationship between the compressive strength, the calcium lactate content and bacterial cell density as well as the age of concrete. This hypothesis holds true when the p-value is less than 0.05 and the $F_{critical}$ is more than the F value, otherwise, the alternate hypothesis (there is a significant relationship between the variables) is adopted. The result is presented in **Table 2**.

Table 2. ANOVA showing the relationship between compressive strength and other variables.

Summary						
Groups	*Count*	*Sum*	*Average*	*Variance*		
Bacteria Conc.	10	1.13E+10	1.13E+09	1E+18		
Calcium lactate	10	10.5	1.05	0.525		
7 days	10	294.3	29.43	20.45789		
28 days	10	388.6	38.86	17.87822		
56 days	10	428.7	42.87	18.19789		
ANOVA						
Source of Variation	*SS*	*df*	*MS*	*F*	*P-value*	*F crit*
Between groups	1.01E+19	4	2.53E+18	12.64045	5.64E-07	2.578739
Within groups	9.01E+18	45	2E+17			
Total	1.91E+19	49				

The result in **Table 2** gives an F value of 12.64045 which is higher than the $F_{critical}$ value of 2.578737. Also the p-value of 5.64×10^{-7} is less than 0.05. In fact, what it means is that there is a less than 0.0001% chance of the null hypothesis being true. The null hypothesis is therefore discarded and the alternate hypothesis is adopted. Namely there is a significant relationship between the parameters. The ANOVA result however does not tell us which parameters have a definite significant relationship. To identify that, a post hoc test is carried out to identify the extent of the relationship between the variables. The true relationship between the variables is determined using the post hoc test known as the Bonferroni and Holm multiple comparison tests, where A, B, C, D and E are the Bacteria Density, Calcium lactate (nutrient content), 7 days, 28 and 56 days' Compressive strengths respectively, and the result is presented in **Table 3**. It can be seen that there is a positive and significant relationship between the bacteria density and each of the other parameters as expected, with both the Bonferroni and Holm P-values less than 0.01 in those relationships. There are however no significant relationships between B and C, B and D, B and E, C and D, C and E as well as D and E, with the p-values well above 0.05. The result of the statistical tests agrees with the experimental result.

3.2 Sorptivity relationship

The relationship between the rate of permeation of substances through the concrete with the age of concrete, bacteria density and nutrient concentration was evaluated using the sorptivity of the concrete. The result is presented in **Figure 2** and it can be seen that the rate of water absorption decreases as the concrete ages, with the 56 days concrete showing better sorptivity than the 7 days concrete.

Also, for each age of concrete, the rate of water absorption (sorptivity behavior) decreased as the bacteria cell density and nutrient concentration increased. This can be seen with the trendlines in **Figure 2**.

The reduction of pore size as a result of calcium carbonate deposition is the main reason for reduced water absorption through the interconnected pores. The reduction in sorptivity with additional calcium lactate (calcium source) and bacterial concentration is due to the additional calcium lactate acting as a catalyst for further deposition of calcium carbonate [13,14].

The filling of the pores by the products of cement hydration as well as the products of the pozzolanic reaction could also account for some reduction in the sorptivity, hence the reduced absorption by S0 with age even though it contains no bacteria and nutrients [15-18]. The statistical relationship between the sorptivity,

Table 3. Bonferroni and Holm significance test.

treatments pair	Bonferroni and Holm T-statistic	Bonferroni p-value	Bonferroni inference	Holm p-value	Holm inference
A vs B	5.6215	1.1346e-05	** p<0.01	1.1346e-05	** p<0.01
A vs C	5.6215	1.1346e-05	** p<0.01	7.9425e-06	** p<0.01
A vs D	5.6215	1.1346e-05	** p<0.01	9.0771e-06	** p<0.01
A vs E	5.6215	1.1346e-05	** p<0.01	1.0212e-05	** p<0.01
B vs C	0.0000	9.9999998	Insignificant	5.9999999	Insignificant
B vs D	0.0000	10.0000000	Insignificant	3.0000000	Insignificant
B vs E	0.0000	10.0000000	Insignificant	1.0000000	Insignificant
C vs D	0.0000	9.9999999	Insignificant	3.9999999	Insignificant
C vs E	0.0000	9.9999998	Insignificant	4.9999999	Insignificant
D vs E	0.0000	10.0000000	Insignificant	2.0000000	Insignificant

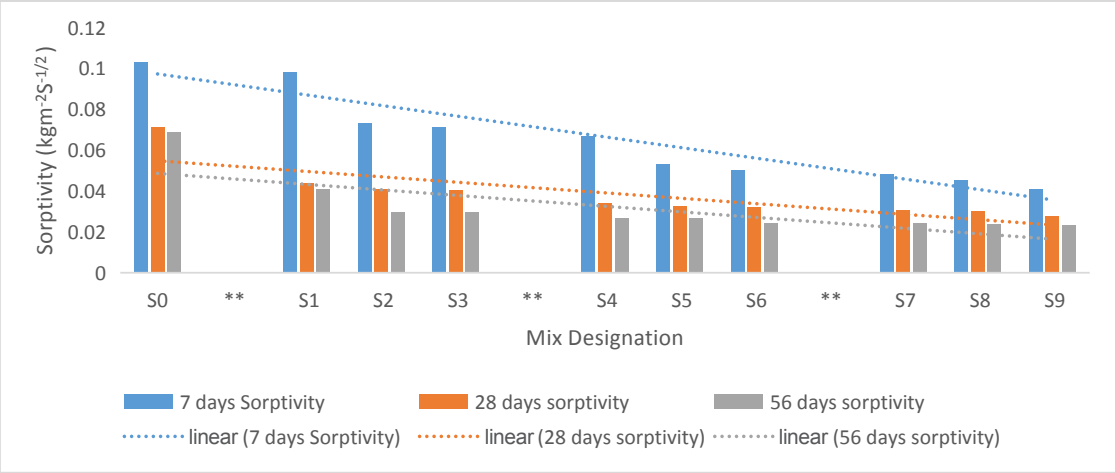

Figure 2. Variation of sorptivity with concrete properties.

age of concrete, bacteria cell density and calcium lactate concentration is evaluated using one-way ANOVA and the result is presented in **Table 4**.

The null hypothesis postulates that there is no significant relationship between the variables and within them, while the alternate hypothesis postulates a significant relationship. As can be seen from **Table 4**, the null hypothesis does not hold because the P-value is less than 0.05. The p-value of 5.64×10^{-7} shows that there is almost no probability of the null hypothesis being true, and it is thus discarded. This is further confirmed by the F value (12.64045) being far more than the critical value of 2.578739. The alternate hypothesis is thus accepted that there is a significant relationship between and within the variables under investigation. A post hoc test carried out to determine where the exact relationships lie using Scheffé's multiple comparisons is given in **Table 5**.

It can be seen that Scheffé's p-value of less than 0.01 holds true for the relationship between bacteria content and nutrient concentration as well as the age of the concrete. There however exists no significant relationship between the nutrient content and the sorptivity at different ages or within the sorptivity at different ages. It has been shown that the effect of nutrients is restricted to it being used up by the bacteria to deposit calcium calcite. This result agrees with the result of the experimental program presented earlier [19].

Table 4. Result of one-way ANOVA for sorptivity.

Summary						
Groups	*Count*	*Sum*	*Average*	*Variance*		
Bacteria Conc.	10	1.13E+10	1.13E+09	1E+18		
Calcium lactate	10	10.5	1.05	0.525		
7 days	10	0.651	0.0651	0.000476		
28 days	10	0.383	0.0383	0.000161		
56 days	10	0.3171	0.03171	0.000196		
ANOVA						
Source of Variation	*SS*	*df*	*MS*	*F*	*P-value*	*F crit*
Between groups	1.01E+19	4	2.53E+18	12.64045	5.64E-07	2.578739
Within groups	9.01E+18	45	2E+17			
Total	1.91E+19	49				

Table 5. Scheffé's post hoc test on sorptivity.

treatments pair	Scheffé T-statistic	Scheffé p-value	Scheffé inference
A vs B	5.6215	6.5174e-05	** p<0.01
A vs C	5.6215	6.5174e-05	** p<0.01
A vs D	5.6215	6.5174e-05	** p<0.01
A vs E	5.6215	6.5174e-05	** p<0.01
B vs C	0.0000	1.0000000	Insignificant
B vs D	0.0000	1.0000000	Insignificant
B vs E	0.0000	1.0000000	Insignificant
C vs D	0.0000	1.0000000	Insignificant
C vs E	0.0000	1.0000000	Insignificant
D vs E	0.0000	1.0000000	Insignificant

3.3 Tensile strength relationships

The relationship between bacteria cell density, nutrient content and tensile strength at 7 and 28 days is plotted in **Figure 3**, As expected, the variation in tensile strength with curing age, bacteria concentration and nutrient content takes the same trend as the compressive strength. This is because of the positive correlation between compressive and tensile strengths [20]. The same explanation for this trend holds for tensile strength as earlier explained for compressive strength.

The result of the ANOVA test to determine the possibility of a significant relationship between the bacteria content, calcium lactate content, and the tensile strength at 7 and 28 days is given in **Table 6**, with the null hypothesis postulating that there is no significant correlation between the bacteria content, the nutrient content and the tensile strength at 7 and 28 days.

The F value (12.64045) is far greater than the F

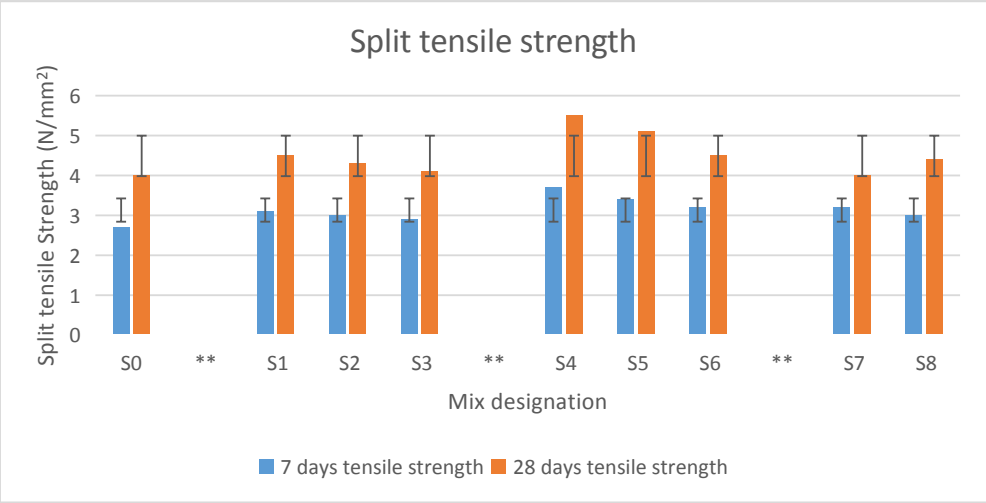

Figure 3. Tensile strength testing.

Table 6. ANOVA test on tensile strength.

Summary						
Groups	*Count*	*Sum*	*Average*	*Variance*		
Bacteria Conc.	10	1.13E+10	1.13E+09	1E+18		
Calcium lactate	10	10.5	1.05	0.525		
7 days	10	31.1	3.11	0.081		
28 days	10	44.41	4.441	0.25281		
ANOVA						
Source of Variation	*SS*	*df*	*MS*	*F*	*P-value*	*F crit*
Between groups	9.49E+18	3	3.16E+18	12.64045	8.51E-06	2.866266
Within groups	9.01E+18	36	2.5E+17			
Total	1.85E+19	39				

critical (2.866266) and the P-value (8.5×10^{-6}) is far less than 0.05, which means that the null hypothesis is rejected. It means that there is a significant relationship between the bacteria content, the nutrient content and the strength at 7 and 28 days.

To determine where the exact relations lie statistically, the Tukey HSD test is carried out on the result of the ANOVA test, using NIST Engineering Statistics Package. The result is presented in **Table 7**.

Table 7. Tukey HSD result for tensile strength.

Treatments pair	Tukey HSD Q statistic	Tukey HSD p-value	Tukey HSD inference
A vs B	7.1107	0.0010053	** p<0.01
A vs C	7.1107	0.0010053	** p<0.01
A vs D	7.1107	0.0010053	** p<0.01
B vs C	0.0000	0.8999947	Insignificant
B vs D	0.0000	0.8999947	Insignificant
C vs D	0.0000	0.8999947	Insignificant

It can be seen from **Table 7** that there is a significant relationship between bacteria density and the calcite content as well as the strength at 7 and 28 days, with a Tukey P-value of less than 0.01. There is however no significant relationship between the calcium lactate content and the strength at 7 and 28 days and within the strengths. This shows that the bacteria content affects the usage of the calcium lactate as well as the tensile strength development. This is in agreement with results presented earlier.

4. Conclusions

The incorporation of calcite precipitation bacteria into calcined clay and limestone powder blended self-compacting concrete positively impacted the strength and permeation properties of the concrete at all ages. The statistical evaluation using ANOVA and the post hoc tests using the Tukey HSD test and Scheffé, Bonferroni and Holm multiple comparisons show that there is a positive and significant relationship between the bacteria dosage and the nutrient content, as well as the age of concrete and the effect on the concrete properties. The use of *sporosarcina pasteurii* at different bacterial cell densities and calcium calcite concentrations is recommended as it has a positive impact on the strength and permeation properties of the ternary SCC.

Author Contributions

Engr Dr. K. Taku Designed the experiment and supervised the Laboratory work and proofreading and correction of the draft manuscript

Engr. T. Agber carried out some of the laboratory work to generate the data as well as wrote the draft Manuscript.

Engr Dr. B. H. S. Amartey supervised the experimentation, carried out the statistical design as well proofread and corrected the manuscript.

Conflict of Interest

There is no conflict of interest.

References

[1] Hasanzadeh, B., Sun, Z., 2019. Impacts of diatomaceous earth on the properties of cement pastes. Journal of Building Materials and Structures. 5(2), 197-211.
DOI: https://doi.org/10.5281/zenodo.2538094

[2] Taku, J.K., Amartey, Y.D., Ejeh, S.P., et al., 2021. Durability evaluation of calcined clay and limestone powder blended ternary self-compacting concrete. Journal of Engineering Sciences. 8(1), C1-C10.
DOI: https://doi.org/10.21272/jes.2021.8(1).c1

[3] Lara, C.R., Diaz, A.A., Scrivener, K., et al., 2011. Study of the addition of calcined clays in the durability of concrete. Revista Ingenieria de Construccion. 28(1), 25-40.

[4] Ma, L., Pang, A.P., Luv, Y., et al., 2020. Beneficial factors for bio-mineralization by ureolytic bacteria *Sporosarcina pasteurii.* Microbial Cell Factories. 19(1), 1-12.
DOI: https://doi.org/10.1186/s12934-020-1281-7

[5] Karihaloo, B.L., Ghanbari, A., 2012. Mix proportioning of self-compacting high- and ultra-high-performance concretes with and without steel fibres. Magazine of Concrete Research.

64(12), 1089-1100.
DOI: https://doi.org/10.1680/macr.11.00190

[6] Deeb, R., Karihaloo, B.L., 2013. Mix proportioning of self-compacting normal and high strength concretes. Magazine of Concrete Research. 65(9), 546-556.

[7] Ghanbari, A., Karihaloo, B.L., 2009. Prediction of the plastic viscosity of self-compacting steel fibre reinforced concrete. Cement and Concrete Research. 39(12), 1209-1216.

[8] BS EN 12390-3, 2009. Testing Hardened Concrete. Compressive Strength of Test Specimens. BSI: London.

[9] BS EN 12390-6, 2009. Testing Hardened Concrete. Tensile Splitting Strength of Test Specimens. BSI: London.

[10] ASTM C1585-13, 2013. Standard Test Method for Measurement of Rate of Absorption of Water by Hydraulic-Cement Concretes. ASTM International: West Conshohocken, PA.

[11] Vaezi, M., Zareei, S.A., Jahadi, M., 2020. Recycled microbial mortar: Effect of bacterial concentration and calcium lactate content. Construction and Building Materials. 234, 1-12.

[12] Irvan, J.M., Teddy, T., 2017. An overview of bacteria concrete on concrete durability in aggressive environment. Pertanika Journal of Science and Technology. 25(5), 259-264.

[13] Mondel, S., Ghosh, A.D., 2018. Investigation on the optimal bacteria concentration for compressive strength enhancement of microbial concrete. Construction and Building Materials. 142, 202-214.

[14] Chahal, N., Siddique, R., Rajor, A., 2012. Influence of bacteria on the compressive strength, water absorption and rapid chloride permeability of concrete incorporating silica fume. Construction and Building Materials. 37, 645-651.
DOI: https://doi.org/10.1016/j.conbuildmat.2012.07.029

[15] Pereira de Oliveira, L.A., Gomes, J.P., Pereira, C.N.A., 2006. Study of sorptivity of self-compacting concrete with mineral additives. Journal of Civil Engineering and Management. 12(3), 215-220.
DOI: https://doi.org/10.1080/13923730.2006.9636395

[16] Dhandapani, Y., Vignish, K., Raja, T., et al., 2018. Development of the Microstructure in LC3 Systems and its effect on concrete properties. In: Martirena, F., Favier, A., Scrivener, K. (editors). Calcined Clays for Sustainable Concrete. RILEM Bookseries, vol 16. Springer: Dordrecht. pp. 131-140.
DOI: https://doi.org/10.1007/978-94-024-1207-9_21

[17] Barkat, A., Kenai, S., Menadi, B., et al., 2019. Effects of local metakaolin addition on rheological and mechanical performance of self-compacting limestone cement concrete. Journal of Adhesion Science and Technology. 33(9), 963-985.
DOI: https://doi.org/10.1080/01694243.2019.1571737

[18] Karatas, M., Benli, A., Arslan, F., 2020. The effects of kaolin and calcined kaolin on the durability and mechanical properties of self compacting concrete mortars subjected to high temperatures. Construction and Building Materials. 265, 1-12.
DOI: https://doi.org/10.1016/j.conbuiltmat.2020.1203000

[19] Sravanthi, M., Rao, S.V., Krishnaveni, K., et al., 2022. Studies on compressive strength and microstructural analysis of self-compacting mortars with bacteria. Communications. 24(4), D183-D200.
DOI: https://doi.org/10.26552/com.C.2022.4.D183-D200

[20] Weber, M., Thiele, C., 2018. Correlation between compressive and tensile strength of old concretes: Applicability of the relationship described in EN 1992-1-1. Structural Concrete. 20(1), 483-492.
DOI: https://doi.org/10.1002/suco.201700244

BILINGUAL PUBLISHING GROUP

Journal of Building Material Science

https://journals.bilpubgroup.com/index.php/jbms

ARTICLE

A Theory on Increasing the Heat Transfer Performance of Building Wall

Yu Zhang**, *ShaoLei Sun

Building Design Institute, China Academy of Building Research, Beijing, 100013, China

ABSTRACT

The target of traditional thermal conductivity of wall research is the spatial distribution form. In these studies, the change of thermal conductivity with temperature is neglected. Meanwhile, case studies are always used. This method needs large computation and it is hard to obtain the optimal result. In order to overcome the problems, a new approach has been put forward in this paper. Different from the traditional approach, the new approach solves an inverse problem under the concept of passive ideal energy-saving buildings to obtain the optimal distribution of heat ability with temperature on an external wall. The result for a typical summer day shows the heat ability distribution of a wall in summer is a staircase. It is similar to the heat pipe. It is also found that the optimal heat transfer property of the external wall is closer to the heat pipe when its heat capacity per square meter ($\rho c_p L$) is of extreme value. This study can provide guidance to researchers in building materials.

Keywords: Thermal conductivity; Building envelope; Passive room; Inverse problem; Nonlinear optimization

1. Introduction

Building energy accounts for 1/3 of the energy consumption of total social goods, increasing in these years. In China, the amount for the latter is about 15% and the ratio is increasing [1]. Meanwhile, carbon emission from buildings accounts for nearly half of that from the city [2]. Hence, it is really significant to put more emphasis on the energy-efficient building research. As the external wall separates the indoor and outdoor environment, proper thermal conductivity for it is important to achieve acceptable comfort for building occupants and reduced cooling and heating load.

Asan [3] studied the optimal location of insulation material which can achieve the maximum time lag and minimum decrement factor of outdoor temperature wave and found that placing half of the insula-

*CORRESPONDING AUTHOR:
Yu Zhang, Building Design Institute, China Academy of Building Research, Beijing, 100013, China; Email: sdjyzhq@163.com

ARTICLE INFO
Received: 24 March 2023 | Revised: 11 April 2023 | Accepted: 24 April 2023 | Published Online: 16 May 2023
DOI: https://doi.org/10.30564/jbms.v5i1.5595

CITATION
Zhang, Y., Sun, Sh.L., 2023. A Theory on Increasing the Heat Transfer Performance of Building Wall. Journal of Building Material Science. 5(1): 49-54. DOI: https://doi.org/10.30564/jbms.v5i1.5595

tion in the mid-center plane of the wall and half of it in the outer surface of the wall gives very high time lags and low decrement factors (close to optimum values). Liu [4] studied the heat conduction problem for tightly compressed adjacent layers of plane plates with gradually varying heat conduction coefficients and obtained the effect of spatial distribution form of thermal conductivity on heat transfer property. Chen [5] considered thermal conductivity to vary with space coordinate according to a linear and an exponential law, based on this proposal six second order heat conduction differential equations were set up. The result showed these equations can't describe true variable-conductivity heat conductions problems. Mahlia et al. [6] analyzed the change between thermal conductivity and thickness of material, which obeys a non-linear polynomial function. Zhong and Zhang [7] investigated the transient heat transfer characteristics of building envelope that is made up of two kinds of three-layered structures. The results show that the position and arrangement of the insulation material are of important effect on the decrement factor and the time lag.

The target of traditional research is mainly on the spatial distribution form of thermal conductivity in order to obtain the optimal layout. In these studies, the way of overture is always used. This method has large computation and it is hard to obtain the optimal result.

Because humans can change clothes with the outdoor temperature, buildings are the same. That is to say, the ideal energy-saving building can properly change the thermal properties ($c_p(t)$, $k(t)$) of external wall with its temperature. Based on this, the objectives of the present research are: (1) to put forward an approach for determining the optimal $k(t)$ of external wall (the $c_p(t)$ of external wall is assumed to be a constant in this study); (2) to demonstrate the application of the approach by using an illustrative example; (3) to provide guidance to researchers in building materials.

2. Problem description

The traditional process of space heating or cooling system design for a given building is shown in **Figure 1**. It can not determine the ideal thermal physical properties of building envelope material, the best natural ventilation strategy and the minimal additional energy consumption of the space heating in winter or air-conditioning in summer. In order to overcome these shortcomings, a new method based on the inverse problem is put forward by us, which is shown in **Figure 2**.

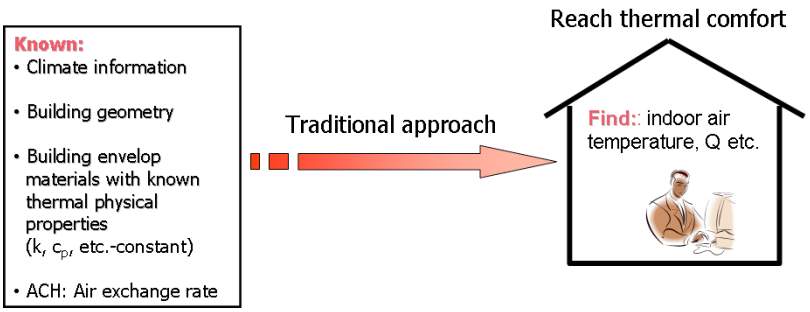

Figure 1. Schematic diagram of the traditional approach.

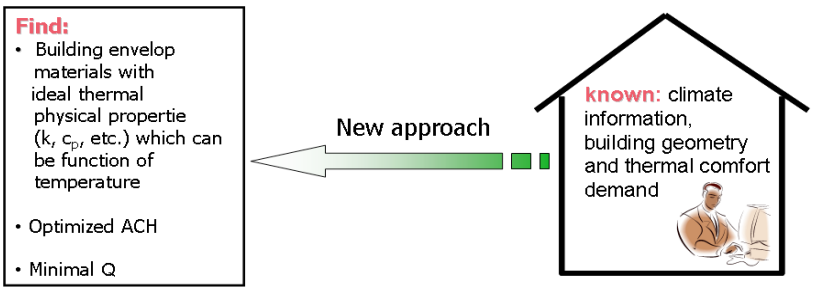

Figure 2. Schematic diagram of the new approach.

For a building that is located in a certain area, having indoor heat, heat ability, *ACH*, and heat ability of wall, the house temperature is the function of external wall heat ability.

$$t_o = f(k_{ew}(t)) \tag{1}$$

where,

$$t_o = \frac{h_r \bar{t}_r + h_c t_a}{h_r + h_c} \tag{2}$$

Integrated uncomfortable degree I [8] can be defined as follows:

$$I_{sum} = \int_{year} (t_o - t_H) d\tau \text{ When } t_o > t_H \tag{3}$$

$$I_{win} = \int_{year} (t_L - t_o) d\tau \text{ When } t_o < t_L \tag{4}$$

where, t_L = 16 °C ,t_H =28 °C.

Combining Equations (1)-(4), we have:

$$I_{sum} = f(k_{ew}(t)) \tag{5}$$

$$I_{win} = f(k_{ew}(t)) \tag{6}$$

As described before, the objective of the inverse analysis is to get the ideal $k_{ew}(t)$ by minimizing the I_{sum} and I_{win} values.

It is easily understood that the smaller $k_{ew}(t)$ is, the lower I_{win} is in winter. So we only study the optimal $k_{ew}(t)$ in summer.

3. Solution of the problem

3.1 Room model

Using the two-plate model in actual room [8]. The wall, floor, and ceiling are fixing into a plate. The radiations about wave in them are ignored. Another wall is the other plate. The error between simplification two plate model and house model is < 20%. Meanwhile, the heat ability of wall is not the sensitivity for error. So the model can be applied into the research of wall heat ability.

Then, the heat ability of external wall is evenly divided into any segments based on its self temperature in the paper and every segment has a heat ability value. two-plate with $k_{ew}(t)$ room model is developed. In order to validate the model, its calculated results and those directly calculated from Airpak model are compared and the maximum absolute deviation of indoor air temperature is 1 °C. It shows that the two-plate with $k_{ew}(t)$ room model can be used to determine the optimal $k_{ew}(t)$.

3.2 Nonlinear optimization method

Obtaining the optimization nonlinear model

Optimization goal: min I (k_1, k_2, k_3,...,k_N)

Restrictive condition: $k_{min} \le k_i \le k_{max}$ (i = 1,2,3,...,N)

As the known insulation materials used in wall, the thermal conductivity k_{min} is 0.02 W/(m·°C). According to analysis, on a typical summer day, it is found that, when the heat ability of the external wall is 35 W/(m·°C), the internal temperature values of the external wall are close to the same. Therefore, the 35 W/(m·°C) is large enough for the external wall thermal conductivity, and k_{max} is set to 35 W/(m·°C) of this paper.

To use the Sequential Quadratic Programming (SQP) method is used to the aforementioned non-linear problem.

4. Illustrative example: Results and discussion

4.1 The calculated conditions

An ordinary passive room in a multi-stories building in Beijing is analyzed. The dimensions of the simulated room are 5.7 m (depth) × 3.6 m (width) × 3.2 m (height). It has an external south-facing wall, and the thickness is 250 mm. The volume heat capacity of the external south-facing wall is 2.3 MJ/(m^3·°C) (180-mm-thick reinforced concrete and 70-mm-thick polystyrene board external wall are used as comparison case). A 1.7 m × 2.0 m double-glazing window is fixed in the exterior south wall. The overall heat transfer coefficient of the double-glazing window is about 3.1 W/(m^2·°C). The shading coefficient (*SC*) value of the window is 0.44 when the window is hung with curtain in summer. The thickness of three concrete hollow block internal walls, reinforced con-

crete floor and ceiling are all 200 mm.

The *ACH* is assumed to be 0.5 h^{-1} when the window is closed. However, the window is open to make full use of the summer night ventilation if the outdoor temperature is lower than 26 °C and higher than 20 °C then the *ACH* becomes 5.0 h^{-1}. The average indoor heat source from people, lights and equipment is about 10.8 W/m^2.

4.2 Results and discussion

The result of a typical summer day shows, the optimal thermal conductivity distribution of the external wall on a typical summer is a staircase function (see **Figure 3**).

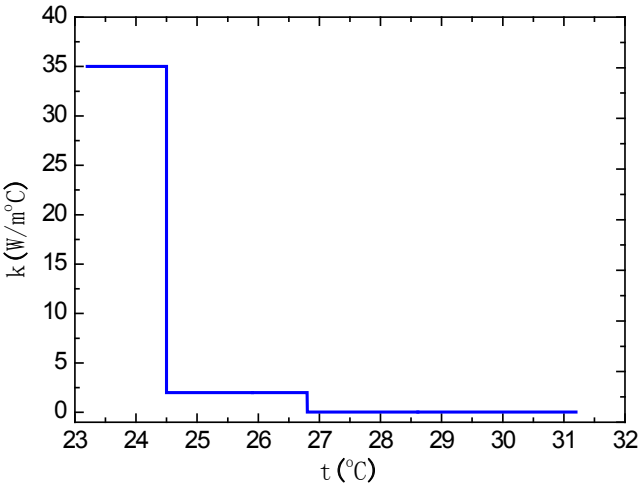

Figure 3. Optimal thermal conductivity distribution of external wall (Beijing, a typical summer day).

The integrated uncomfortable degree is reduced by 99% by optimization and the optimized highest indoor operative temperature is 1 °C lower.

The physical mechanism can be explained as follows: In summer, there are two heat transfer directions in the external wall. When the temperature of the external wall is lower, it plays a role in cooling indoor environment and heat transfer direction in it is from indoor side to outdoor side. At this moment, large thermal conductivity is helpful to reduce indoor temperature. When the temperature of external wall is higher, it plays a role in heating indoor environment and heat transfer direction in it is from outdoor side to indoor side. At this moment, small thermal conductivity is helpful to avoid exaltation of indoor temperature. So ideal $k_{ew}(t)$ is that large thermal conductivity lies in the low temperature region and small thermal conductivity lies in the high temperature region. Meanwhile, there exists an overlap region where thermal conductivity is a certain value which depends on the calculation case.

It is seen that the optimal heat transfer property of external wall is similar with the function of heat pipe from **Figure 1**. When the overlap temperature region is zero, they are the same. The reason is that when we see an external wall as a heat pipe with large thermal conductivity in the direction from indoor to outdoor and small thermal conductivity in the direction from outdoor to indoor, there are two heat transfer directions in the external wall. When the temperature of the external wall is low, the outdoor temperature is lower than the indoor temperature (because there is indoor heat source), so the temperature of inner surface of the external wall is higher than that of exterior surface of the external wall and the heat transfer direction in the external wall is from indoor to outdoor. At this time, the thermal conductivity of the external wall is large. On the contrary, when the temperature of the external wall is high, the outdoor temperature is higher than the indoor temperature (because the intensity of indoor heat source is not so large), so the temperature of exterior surface of the external wall is higher than that of inner surface of the external wall and the heat transfer direction in the external wall is from outdoor to indoor. At this time, the thermal conductivity of the external wall is small. This is the same with optimization result without overlap temperature region. As the overlap temperature region accounts for a less proportion in the actual optimization result, heat pipe can be considered to be applied in the design of optimal performance of the external wall.

Then, dimensionless analysis is carried out for an external wall, and three natural physical parameters (ρc_p, *L*, *k(t)*), which are representative of the performance of wall, are obtained. **Figure 4** shows optimization results for thermal conductivity distribution of the external wall on a typical summer day with

different ρc_p. It is seen that: (1) I_{sum} decreases after optimization and decreases with increasing ρc_p; (2) I_{sum} is almost zero when ρc_p is over 2.3 MJ/(m^3·°C). That is to say, for the case considered, 2.3 MJ/(m^3·°C) is the critical value of ρc_p for free-cooling building in Beijing; (3) The width and height of overlap temperature region increases and lower temperature is contained in the overlap temperature region with increasing ρc_p. It means that the optimal heat transfer property of the external wall is closer with heat pipe when its ρc_p is of the extreme value. The reasons for the above phenomena are as follows: The ability of the external wall increases increasing ρc_p, so its ability to adjust indoor temperature increases and I_{sum} will reduce. Meanwhile, with increase of ρc_p, the internal temperatures of the external wall raise less in summer. As a result, the overlap temperature region contains lower temperatures and internal temperatures of the external wall are more likely to simultaneously exist in heat transfer process in both directions of the external wall which causes the increasing width of overlap temperature region. Since the external wall has the function of giving out heat to the outdoor environment on a typical summer day, when ρc_p is infinity, the temperature of the external wall keeps unchanged and the temperature of inner surface is higher than that of exterior surface. Under this conduction, the ideal $k_{ew}(t)$ should also be infinity. So the height of overlap temperature region will increase until the maximum is obtained.

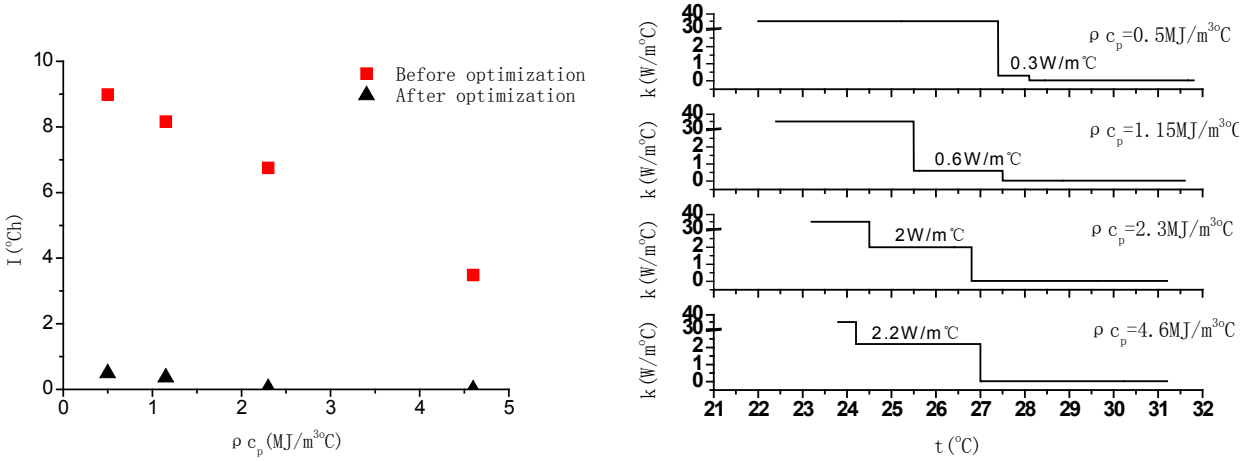

Figure 4. Optimization results in a typical summer day with different ρc_p (L = 0.25 m).

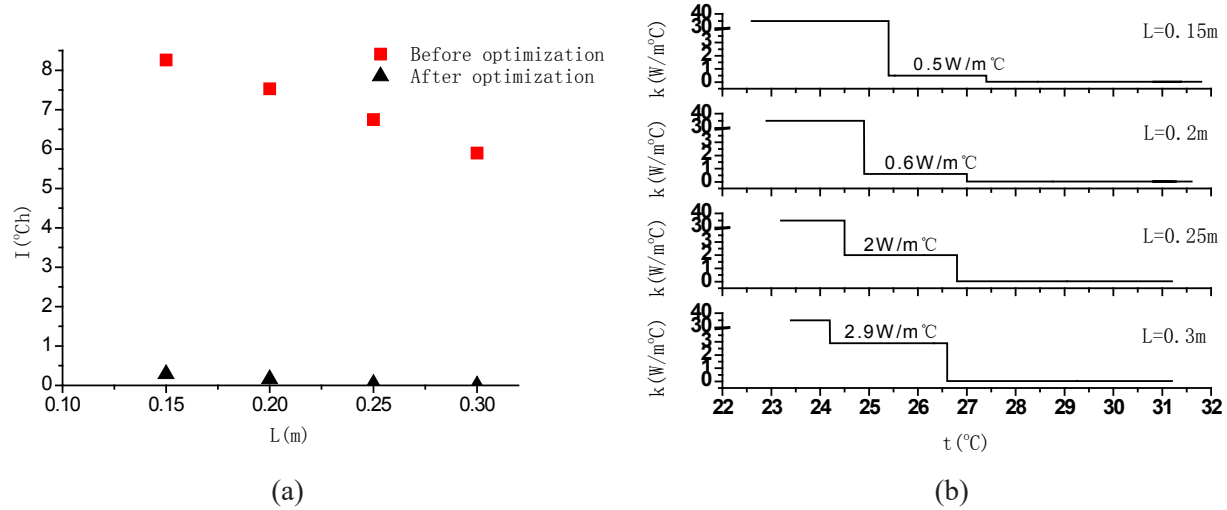

Figure 5. Optimization results in a typical summer day with different L (ρc_p =2.3 MJ/(m^3·°C)).

Figure 5 shows optimization results for heat ability of the external wall on a typical summer day with different L. It is seen that: (1) I_{sum} decreases after optimization and decreases with increasing L; (2) I_{sum} is almost zero when L is over 0.2 m. So for the case studied, $L > 0.2$ m can meet the requirements of free-cooling building in Beijing; (3) The width and height of overlap temperature region increases and lower temperature is contained in the overlap temperature region with increasing L. It means that the optimal heat transfer property of the external wall is closer to heat pipe when its L is of the extreme value. The reason for (1) is that the ability of heat insulation of the external wall increases with increasing L, so I_{sum} will reduce. The reasons for (2), (3) are the same as that mentioned above.

5. Conclusions

In this paper, a new approach for developing energy efficient buildings is put forward. An illustrative example of applying it is presented. The results show that:

(1) The optimal heat ability distribution of the external wall in a typical summer day is a staircase function.

(2) ρc_p and L has no effect on the form of optimal thermal conductivity distribution of the external wall, only existing certain stretching and offset.

(3) Heat pipe is more appropriate in the application of the design of optimal performance of the external wall when $\rho c_p L$ of the external wall is of the extreme value. It can provide guidance to researchers in building materials.

Author's Contributions

Yu Zhang presented a solution to the problem known as the inverse problem method of the wall.

ShaoLei Sun established the room model and calculated the case.

Conflict of Interest

There is no conflict of interest.

References

[1] Tsinghua University Buildings Energy Efficiency Research Center, 2009. 2009 zhong guo jie neng bao gao (Chinese) [Annual report on China building energy efficiency]. TUBEERC: Beijing.

[2] Wang, Zh.Y., Tang, F.X., 2010. Di tan jian zhun chui xiang chong feng hao jiao (Chinese) [Low carbon buildings blow bugle call to charge]. China High Technology Enterprises. (26).

[3] Asan, H., 2000. Investigation of wall's optimum insulation position from maximum time lag and minimum decrement factor point of view. Energy and Buildings. 32(2), 197-203.

[4] Liu, H., 1981. Re chuan dao xi shu zhu jian bian hua de ban dao re wen ti (Chinese) [Heat conduction problem for tightly compressed adjacent layers of plane plates with gradually varying heat conduction coefficients]. Applied Mathematics and Mechanics. (2).

[5] Chen, G.Q., 1992. Bian re dao jie zhi wei fen fang cheng ji qi yi yi (Chinese) [On the differential equations and its meaning for variable-conductivity medium]. Journal of Shaoyang College. (2).

[6] Mahlia, T.M.I., Taufiq, B.N., Masjuki, H.H., 2007. Correlation between thermal conductivity and the thickness of selected insulation materials for building wall. Energy and Buildings. 39(2), 182-187.

[7] Zhong, Z.P., Zhang, Y.P., 2000. Optimal arrangement of the insulation layer in a three-layered wallboard. Heat Transfer Science and Technology 2000, 2000, 867-872.

[8] Zeng, R.L., Wang, X., Di, H.F., et al., 2011. New concepts and approach for developing energy efficient buildings: Ideal specific heat for building internal thermal mass. Energy and Buildings. 43, 1081-1090.

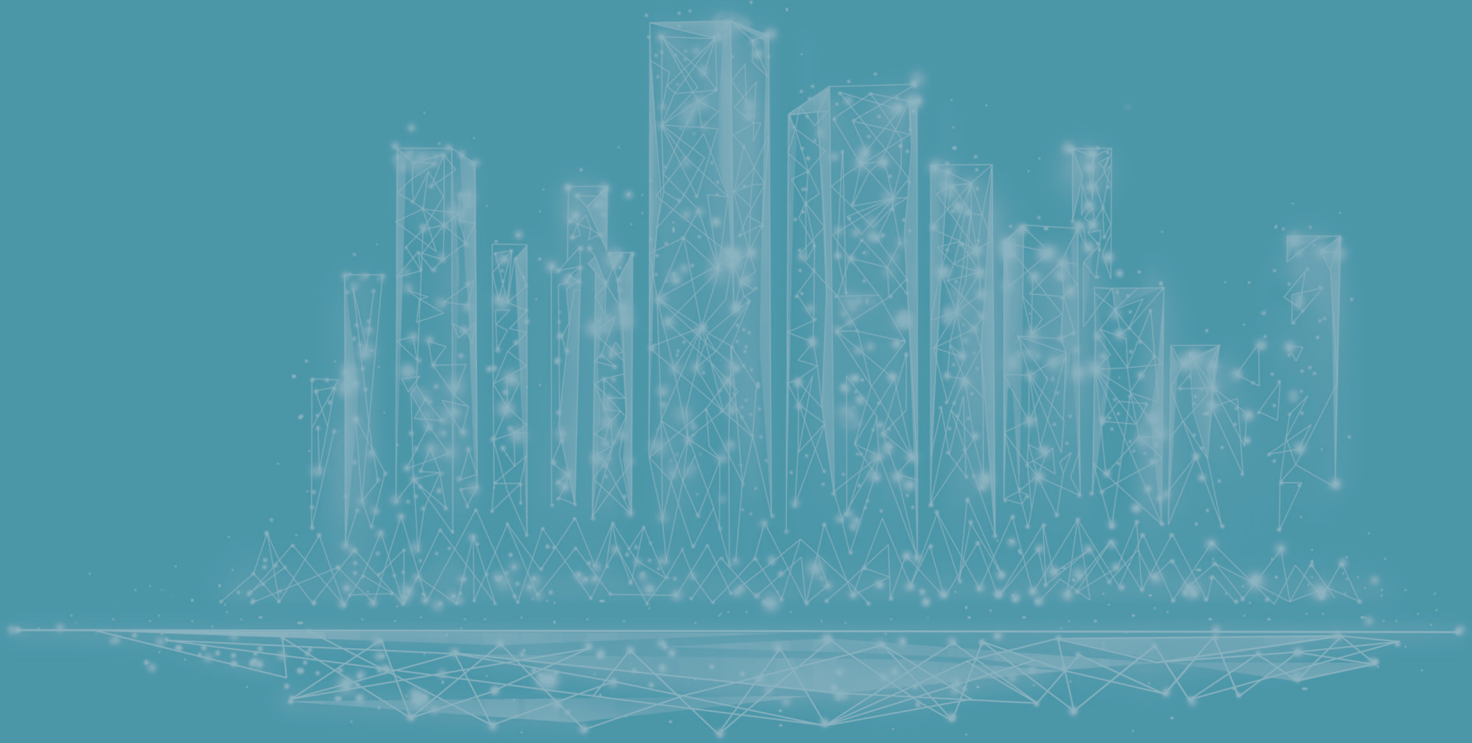

BILINGUAL PUBLISHING GROUP

Tel:+65 65881289
E-mail: contact@bilpublishing.com
Website:https://journals.bilpubgroup.com

2630-5216 01
9 772630 521231